Distribution Agreement

In presenting this thesis or dissertation as a partial fulfillment of the requirements for an advanced degree from Emory University, I hereby grant to Emory University and its agents the non-exclusive license to archive, make accessible, and display my thesis or dissertation in whole or in part in all forms of media, now or hereafter known, including display on the world wide web. I understand that I may select some access restrictions as part of the online submission of this thesis or dissertation. I retain all ownership rights to the copyright of the thesis or dissertation. I also retain the right to use in future works (such as articles or books) all or part of this thesis or dissertation.

Signature:

_____   _____
Yulei Cao   Date

Structural Factors of Radical-Enhanced Intersystem Crossing of Organic Chromophores

By

Yulei Cao
Master of Science

Chemistry

Tianquan Lian, Ph.D
Advisor

Craig Hill, Ph.D
Committee Member

Francesco Evangelista, Ph.D
Committee Member

Nichole Powell, Ph.D
Committee Member

Accepted:

Lisa A. Tedesco, Ph.D
Dean of the James T. Laney School of Graduate Studies

Date

Structural Factors of Radical-Enhanced Intersystem Crossing of Organic Chromophores

By

Yulei Cao

Advisor: Tianquan Lian, Ph.D

An abstract of
A dissertation submitted to the Faculty of the
James T. Laney School of Graduate Studies of Emory University
in partial fulfillment of the requirements for the degree of
Master of Science
in Chemistry
2018

Abstract

Structural Factors of Radical-Enhanced Intersystem Crossing of Organic Chromophores

By Yulei Cao

A long-lived triplet state is essential for various applications such as triplet-triplet annihilation upconversion, photodynamic therapy, and photocatalysis. Current research on efficiently generating long-lived triplet states mainly depends on the heavy atom effect, which limits the applications of triplet sensitizers in the biomedical field. Although triplet generation via radical enhanced intersystem crossing (EISC) of organic chromophores has been reported, discrepancies exist among different studies. In this project, we synthesized and measured the intersystem crossing (ISC) rate of boron dipyrromethene (BODIPY) with a 2,2,6,6-tetramethyl-1-piperidinyloxyl (TEMPO) radical attached at different positions or with different distances. Anthracene (ACA)-TEMPO was also examined. The BODIPY results indicate a distance dependent radical EISC effect. The BODIPY-TEMPO molecule with a short rigid linker presented a higher ISC rate and a longer-lived triplet state, which was observed for the first time. The comparison between a short rigid and a long flexible linker revealed a through-bond effect of the radical EISC process. This work contributed to the finding of how radicals enhance intersystem crossing.

Structural Factors of Radical-Enhanced Intersystem Crossing of
Organic Chromophores

By

Yulei Cao

Advisor: Tianquan Lian, Ph.D

A dissertation submitted to the Faculty of the
James T. Laney School of Graduate Studies of Emory University
in partial fulfillment of the requirements for the degree of
Master of Science
in Chemistry
2018

Acknowledgement

Table of Content

List of Figures

List of Tables

List of Schemes

Chapter 1. Introduction

1.1 Overview

Molecular engineering is the modification of electronic, spatial, and molecular structure, which allows the tuning of photonic and electronic properties, leading to various applications. Organic molecules, due to their larger and more flexible structures, are generally more tunable. In many molecular engineering designs, the attachment of organic radicals is interesting because of the intriguing phenomenon of the free spinning single electron of radicals. One of its applications is enhanced intersystem crossing (EISC). Singlet excited state to triplet state intersystem crossing (ISC) has been a popular area of study over the years due to the utilization of triplet state molecules in diverse fields, such as renewable energy and defense supplies. Radical EISC of organic chromophores was recently observed, yet disparities appeared among different compounds due to the flexibility of organic molecules. Charge transfer between radical and chromophore, a process that competes with ISC during molecular relaxation, is another noticeable chemical property since it demonstrates the relocation of electrons and allows the analysis of photocatalytic and photoinduced charge separation processes. Thus, investigating the radical EISC and charge transfer process in different chromophore-radical systems will provide insightful understanding, and lead to the development of the molecular design of optimal EISC.

1.2 Triplet State and Intersystem Crossing

Solar energy is one of the main sources of renewable energy. Currently, the widely used solar cell material utilizes a small portion of sunlight, the high-energy blue-to-ultraviolet (UV)[1] part of the spectrum. One of the approaches to enhance the solar cell efficiency is through the use of triplet photosensitizers[2]. Triplet photosensitizers are compounds with high intersystem crossing rates, long-lived triplet states, and strong absorption in the visible light region[2]. Triplet photosensitizers have various important applications such as triplet-triplet annihilation upconversion[3], photodynamic therapy[4], and photocatalysis[5]. For example, photodynamic therapy relies on the long-lived triplet state of the photosensitizer[2, 4, 6]. Upon illumination, the chromophore photosensitizer absorbs a photon to reach to the singlet excited state, then this state converts to triplet via intersystem crossing (ISC)[4]. Relaxation from triplet state to ground state is coupled with the excitation of oxygen from ground state triplet to excited state singlet. Singlet oxygen in tissues has a short lifetime and a limited diffusion distance, and thus photodynamic therapy can target a specific area without affecting normal, neighboring cells[4]. This property allows photodynamic therapy to be widely applied in tumor and cancer treatments. The design and synthesis of an efficient and sensitive photosensitizer has been a major area of study. One of the difficulties in photodynamic therapy relates to the limited ISC rate[6]. Since the oxygen concentration in body tissue is limited, a low ISC rate will restrict the triplet population of the photosensitizer, and as a result, restrain the generation of singlet oxygen and reduce the effect of

treatment.

Another application of triplet molecules is photocatalysis. The triplet excited state electron is able to easily leave the molecule, and the single electron remaining in the ground state is also likely to accept an electron from outside of the molecule. Because of these characteristics, a triplet state molecule is both a strong oxidant and strong reductant. In addition, the long-lived triplet excited state creates a higher possibility for a reaction to occur. Thus, as a triplet photosensitizer is excited by photon and achieves a triplet state through intersystem crossing, it is able to catalyze various types of reactions, a process known as photocatalysis. One of the popular and most investigated visible-light photocatalyst currently uses ruthenium and iridium with aromatic ring complexes[7]. Upon photonexcitation, electron transfer from the metal centered orbital to ligand centered orbital (metal-to-ligand charge transfer or "MLCT") takes place. This single LMCT excited state rapidly undergoes intersystem crossing to a lower energy triplet MLCT state. The transition from a triplet excited state to ground state is a spin forbidden process, which allows the triplet state to be long-lived, and consequently facilitates a reduction or oxidation reaction to take place[7]. While ruthenium and iridium photocatalysts are effective, medicinal chemists aim to develop photocatalysts without heavy atoms, which are generally judged to be safer when applied to biological systems. The organic radical, 2,2,6,6-tetramethylpiperidinyloxy (TEMPO), was one of the compounds investigated as a co-catalyst for a photoredox reaction[8].

Intersystem crossing is a process during which an electron shifts between two electronic

states with different spin multiplicities[3]. Due to the wide application of a long-lived triplet state, the singlet-triplet ISC is an important area of study. ISC involves spin change, and thus this process is forbidden[9] (Figure 1). Current research approaches this problem mainly by developing organometallic compounds such as triplet photosensitizers[6]. The free spinning heavy metal atom assists the ISC process and generates a long-lived triplet state[5]. However, this introduces a big splitting in energy between singlet and triplet state, which limits the number of available acceptor. In addition, heavy atoms are frequently highly toxic, therefore, introducing a heavy atom creates difficulties and limitations for in-vivo applications of triplet photosensitizers in areas such as biochemical imaging and photodynamic therapy for cancer treatment[6]. Thus, developing an EISC method with heavy-atom-free molecules and materials is essential. One of the approaches is introducing an organic radical[3, 10]. Since a radical has a single electron that can easily change its spin, linking radicals with the chromophores maintains a net spin of zero during the intersystem crossing (ISC) of the photosensitizer (Figure 2). This characteristic creates an overall spin-allowed transition, and thus enhances ISC rate.
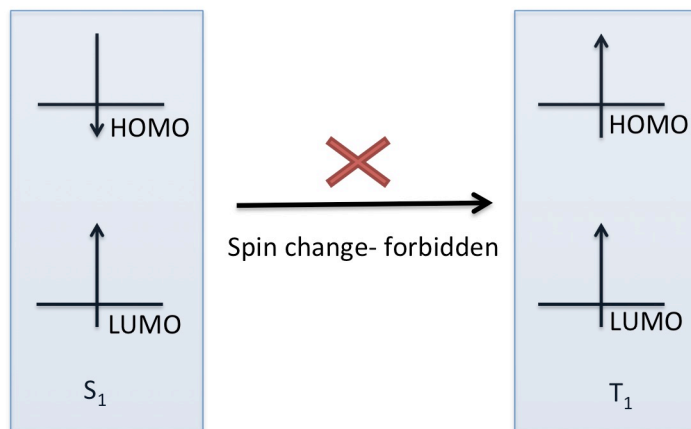
Figure 1: Illustration of the spin forbidden ISC process.
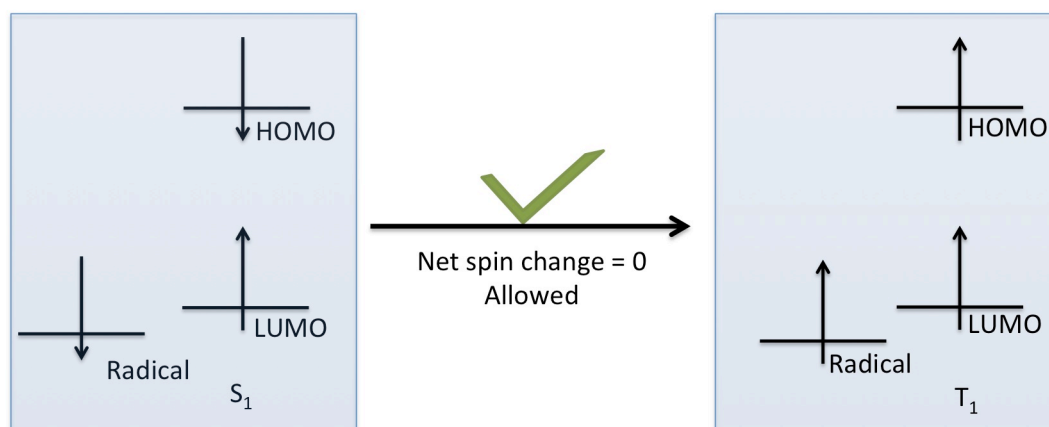
Figure 2: Spin allowed ISC process facilitated by free spinning electron

However, other competing dynamic processes exist which can decrease the radical EISC process, and electron transfer is one example. Electron transfer is a dynamic process in which an electron relocates from one molecule to another, generally involving oxidation or reduction reaction[10]. In the organic-radical system, electron transfer competes with intersystem crossing and creates an oxidized or reduced radical-chromophore compound, which allows a fast relaxation of molecules from the singlet excited state to the ground state (Figure 3). A solvent dependent radical quenching of an excited singlet state chromosphere via electron transfer has been

observed with the perylene-3,4:9,10-bis(dicarboximide) (PDI)-TEMPO system[10]. PDI is quenched

by EISC in toluene and by electron transfer in tetrahydrofuran (THF)[10]. This charge separation

state is generally undesired due to the chemical properties of the oxidized or reduced species. For

example, in photodynamic therapy, instead of singlet oxygen created by ISC, charge transfer

generates other reactive oxygen species such as superoxide and hydrogen peroxide. These

products have a much longer lifetime and may diffuse and transfer to other regions in the body

and cause damage.

Chromophore-Radical S_1

Chromophore-Radical T_1

Chromophore$^+$ -Radical$^-$
Chromophore$^-$ -Radical$^+$

Chromophore-Radical S_0
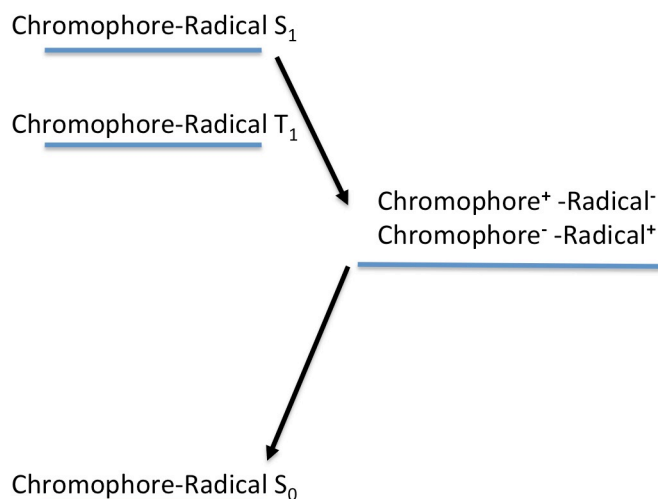
Figure 3: Charge transfer process illustration.

1.3 BODIPY and Derivatives

Despite the fact that photosensitizers are currently undergoing intense study, very few

systems have been developed for radical EISC. Boron dipyrromethene (BODIPY) is one of the

most popular photosensitizers (Figure 4). BODIPY has large fluorescence quantum yield,

indicating a strong radiative decay from the singlet excited state to the ground state. Thus, the ISC of BODIPY molecules with different substituents have been studied by many researchers, and the ISC process proceeds through various mechanisms including the heavy atom effect, spin conversion, and exciton coupling effect[9]. For example, when linked with anthracene, BODIPY generates a locally excited triplet state via photoinduced electron transfer, since the charge separation state facilitated the generation of triplet state[11]. Radical EISC of BODIPY was observed recently. Wang et al. reported the fluorescence of BODIPY was significantly quenched, and the spin-polarized TEMPO signal was observed, which led to an efficient ISC and a long-lived triplet excited state[3]. This literature also investigated the distance dependent effect of radical enhanced ISC, and observed a higher ISC rate and relatively shorter triplet state lifetime with the shorter linker[3].
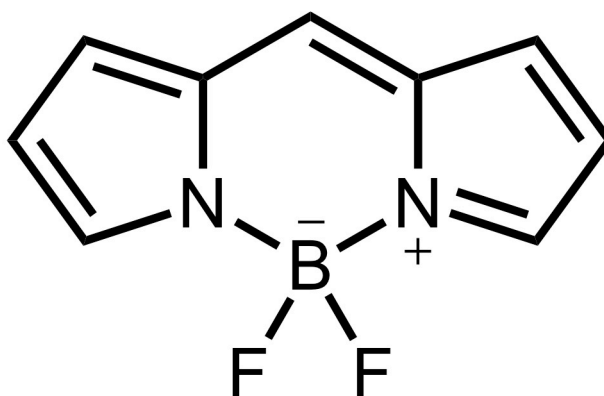
Figure 4: A BODIPY skeleton structure.

1.4 Anthracene and Derivatives

Other organic chromophore systems were also investigated for the radical EISC effect, and

acenes are one of the main areas of study. Acenes are formed by linearly connected benzene rings, which have conjugated electron systems[12]. Since acenes have fundamental structures that can be modified with different substrates, the tunable structural and electronic properties allow acenes to be one of the most studied class of molecules for triplet studies[12]. Theoretically, researchers have found acene systems are longer than pentacene are highly unstable due to their open shell character, in which the highest occupied molecular orbital-lowest unoccupied molecular orbital (HOMO-LUMO) gap was decreased due to unpaired or partially unpaired electrons in the system[13]. Yet, experimentally, longer acenes or oligoacenes are difficult to synthesize since they tend to dimerize or polymerize. Some successful synthetic results show that heptacene and nonacene exhibit closed shell characteristics, which is not what is desired[14]. Recently, a nonacene derivative with open shell singlet property has been developed, and its spectroscopy shows a diradical feature due to the open shell character[15]. Thus, introducing an organic radical to acene molecules may increase the likelihood that the singlet will under ISC to the triplet. Chernick, et al. investigated a pentacene-TEMPO radical system[12]. However, they did not observe an enhanced singlet excited state to triplet excited state ISC rate, while the triplet state was quenched by the TEMPO radical as a function of TEMPO-to-pentacene distance.

1.5 Radical Enhanced Intersystem Crossing of Organic Chromophores

Currently, discrepancies exist among different literatures regarding the effect of radicals on

the ISC rate of organic chromophores. To be specific, a distance-dependent radical EISC was observed with the BODIPY system[3], but not yet in a pentacene system[12]. In addition, when TEMPO was linked with perylene-3,4:9,10-bis(dicarboximide) (PDI), the PDI exhibited an EISC in toluene solvent and a charge transfer process in THF solvent[16]. Also, the TEMPO radical affects ISC when linked to tetra-*tert*-butylphthalocyaninatosilicon (SiPc), and the decrease of triplet lifetime appears to be dependent on the number attached radicals[17]. It is problematic to directly compare these systems since they were measured using different instruments and under different experimental conditions. For example, although the BODIPY system reported EISC[3], the pump pulse used in the transient absorption experiment had an extremely high power. It is possible that this high energy laser fragmentized the molecule, and the decay trace was mistakenly attributed to the triplet lifetime. In addition, several issues remain unclear. First, the distance factor in the literatures[3, 12] refers to the through-bond distance, yet no research addressed whether the distance influence could also be a significant factor. Second, the additive effect was investigated in a structure where the mono- and di- radical were perpendicular to the planer organic chromophore, yet the in-plane attachment geometry was not investigated. Third, different attachment positions of the radical on the same molecule may also be a factor that influences the ISC rate. Thus, in this project, we aim to examine and clarify the ISC effect of the TEMPO radical on different organic chromophores, and to investigate different structural factors in EISC. Our targeted compounds are shown in Scheme 1. BDP-TEMPO-M is the same molecule as investigated in Wang's work[3], and we aim to confirm the unusually long triplet state lifetime as

well as to compare it to BDP-TEMPO-L to investigate the influence of the linkage position on radical EISC. BDP-TEMPO-S has a short through bond linkage, yet the TEMPO radical was not flexible enough to rotate over and create a spatial influence. Thus, comparing BDP-TEMPO-S to BDP-TEMPO-L would allow us to draw a conclusion of whether radical EISC is a through-bond or through-space interaction, as well as provide a distance dependence study on BODIPY-TEMPO with 2, 6 attachment. Anthracene is an organic chromophore with a relatively simple structure. Data for ACA-TEMPO can be compared to the literature for pentacene-TEMPO[12] to investigate the effect of the size of the chromophore conjugated system. It can also be applied to the SiPc system[17] since ACA-TEMPO provides an in-plane radical attachment to the planer chromophore.

Scheme 1: Targeted Organic Chromophore-Radical and related molecules of interest

BDP-TEMPO-M

BDP-TEMPO-L

BDP-TEMPO-S

ACA-SH

ACA-TEMPO
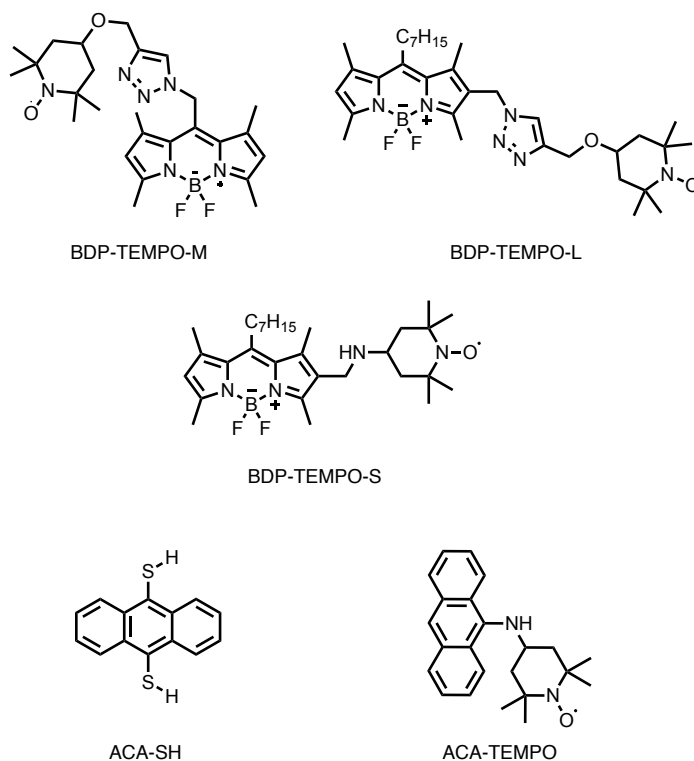
Chapter 2. BODIPY-TEMPO System

2.1 Methods

2.1.1 Synthesis

The starting materials, solvents, and catalysts were purchased from Sigma-Aldrich Chemical Company.   A BODIPY with TEMPO radical connected via the meso position (BDP-TEMPO-M) was prepared (Scheme 2). The synthesis process of compound **1**, **2**, **4**, and BDP-TEMPO-M followed literature methods[3], yet modifications were made for the synthesis of compound 2(BDP-N3). To synthesize BDP-N3, 80 mg of compound **1** (BDP-Cl) was added to a flame-dried, round bottom flask with 52.26 mg (3x equivalent) of sodium azide with 6 ml of THF as solvent and stirred under argon at 45 °C overnight. The product mixture appeared to be orange-red, and the product had an Rf value of 0.8 using 30% ethyl acetate in hexane. After column chromatography with ethyl acetate and hexane, the pure product was a bright red solid and the solution was bright orange-pink. Compound **1**, **2**, and **3** were characterized by proton nuclear magnetic resonance (^{1}H NMR) spectroscopy (600 MHz INOVA) in deuterated chloroform (CDCl$_3$) solution, and BDP-TEMPO-M was characterized by mass spectrometry (LTQ-FTMS).

The preparation of BDP-TEMPO-S and BDP-TEMPO-L were performed by Dr. Yiming Huang from the Egap Lab at Rice University as shown in Scheme 3. Compound **4** and compound **7** followed literature procedure[18]. To prepare compound **5**, NaBH$_4$ (9 mg, 0.24 mmol) was added

to a solution of compound **4** (78 mg, 0.22 mmol) in 25 mL of THF at -78°C, and the mixture was stirred until the starting material was fully consumed by TLC analysis (approx. 4h). The reaction mixture was washed with 1 M HCl, extracted with DCM, and concentrated under vacuum. The crude material was purified by column chromatography (SiO$_2$, hexanes / EtOAc, gradient) to give the product as a red solid (12 mg, 15%). To synthesize compound **6**, a solution of compound **2** (12 mg, 0.033 mmol) in 1 mL of THF at 0 °C was added to 50 μL diphenyl phosphoryl azide and then 50 μL of Et$_3$N. The mixture was stirred at room temperature overnight until the starting material was fully consumed, a reaction again monitored by TLC. The reaction mixture was washed with saturated aqueous NaHCO$_3$, extracted with DCM, and concentrated under vacuum. The crude material was purified by column chromatography (SiO$_2$, hexanes / EtOAc, gradient) to give the product as a red solid (5 mg, 38%).

For BDP-TEMPO-L, a mixture of compound **3** (5 mg, 0.013 mmol), 4-propagyloxy-TEMPO (9 mg, 0.043 mmol), 0.5 mg of CuI, 50 μL of Et$_3$N in 1 mL of THF was stirred at room temperature for 24 h. The reaction mixture was washed with saturated aqueous NaCl, extracted with DCM, and concentrated under vacuum. The crude material was purified by column chromatography (SiO$_2$, hexanes / EtOAc, gradient) to give the product as a red solid (2 mg, 26%). For BDP-TEMPO-S, a mixture of compound **4** (20 mg, 0.053 mmol), 4-amino-TEMPO (20 mg, 0.12 mmol), and 60 mg of neutral alumina was stirred for 48 h before the alumina was filtered off. To the remaining filtrate was added a solution of 5 mg of NaBH$_3$CN in 1 mL of MeOH. The new mixture was stirred for another 3 h, washed with saturated aqueous NaCl, then extracted with

DCM, and concentrated under vacuum. The crude material was purified by column

chromatography (SiO$_2$, EtOAc) to give the product as a red solid (6 mg, 21%).

Scheme 2: Preparation for BDP-TEMPO-M[3]
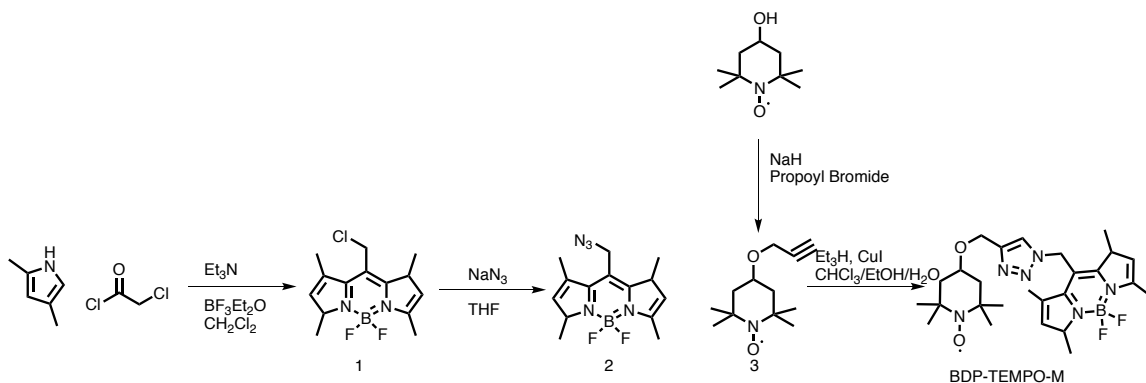
Scheme 3：Synthesis for BDP-TEMPO-L and BDP-TEMPO-S
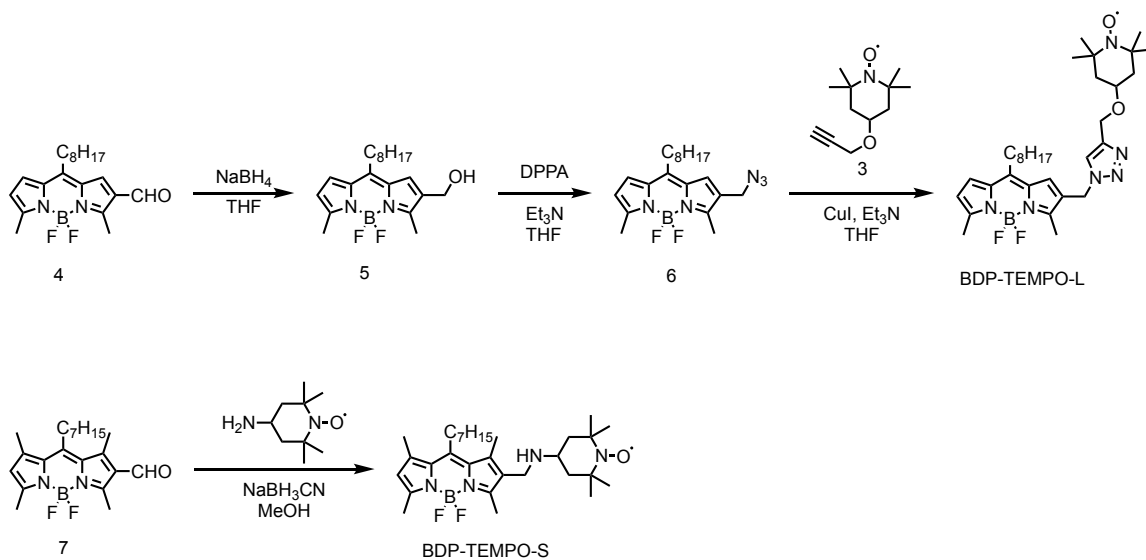
2.1.2 Steady State Absorbance and Fluorescence

UV-Vis absorption spectra for BDP-TEMPO-M and BDP-N3 were measured with Agilent

Cary 60 spectrometer. Steady-state fluorescence emission spectra were measured with Agilent

Cary Eclipse fluorometer with an excitation pulse of 460 nm. Samples were dissolved in toluene

with a concentration of 10^{-5} M, and the solutions were prepared under air at room temperature. Spectral data were processed by Igor Pro, WaveMetrics.

The UV-Vis absorption spectroscopy for BDP-TEMPO-S and BDP-TEMPO-L were conducted using an Agilent 8453 (Agilent Technologies) instrument, and the fluorescence emission spectra were taken by Fluoromax 3 fluorometer with an excitation wavelength of 480 nm. The fluorescence quantum yields of BDP-TEMPO-S and BDP-TEMPO-L were acquired by measuring the absorbance and fluorescence of the samples and a standard, Rhodamine B, at different concentrations. The absorbances of the samples were kept lower than 0.1 OD to avoid re-absorption. The fluorescence spectra at different concentrations were integrated and plotted against photons absorbed. The plots were fitted by a linear function, and the slopes were compared to the standard to determine the fluorescence quantum yields.

2.1.3 Excited State Transient Spectroscopy Study

For transient absorption spectroscopy on all the BODIPY and BDP-TEMPO samples, the samples were dissolved in toluene with a concentration of 10^{-5} M. The solutions were processed with "freeze-pump-thaw" technique to ensure they were oxygen free, and were stored under Ar in a glove box (MBraun). The oxygen concentration in the glove box was recorded as between 15.5-17.5 ppm during the sample preparation times.

Femtosecond transient-absorption spectroscopy was used to produce the picosecond level excited state dynamics. The transient spectroscopy experiment followed the general setup from

our lab[19-20]. To be specific, the laser beams were generated by Ti:sapphire laser system (Coherent Legend), with a central wavelength of 800 nm, a pulse duration of 150 fs, a repetition rate of 1 kHz, with 2.4 mJ/pulse. The 800-nm output pulse was separated into two parts with 90:10 ratio to generate a pump beam (90%) and a white light continuum (10%). A part of the output for pump beam generation (1mJ, 800nm) was split into the Optical Parametric Amplifier (Opera, Coherent), which generates signal and idler, two tunable pulses ranged from 1.1-2.5 μm. A dichroic mirror was used to separate the signal and idler beams. For BODIPY related compounds, the pump beam was set to 500 nm by sum frequency generation of the signal pulse at 1333 nm and the fundamental 800-nm pulse in a barium borate (BBO) crystal. A band pass filter was added to filter assembly out the remaining near-infrared (NIR) pulse and the 800 nm pulse. To provide the spectroscopic data of the unexcited state signal, a chopper synchronized to 500Hz was applied to block every other pump pulse. The sample solution was contained in a quartz cell with 1 mm pathlength and 1 cm width. A stir bar was used to avoid photodegradation of the sample. The pump beam was aimed at the sample with a beam width of 400 μm. The white light continuum was produced by pointing the split part of 800 nm laser beam into CaF_2 windows for UV region, providing light with wavelength from 360-880 nm, which was divided again into probe (70%) and reference (30%) beams. An Al parabolic reflector was used to focus the probe light onto the sample cell at about 100 μm beam waist, and the reference and probe signal were collected by a fiber-coupled multichannel spectrometer. The optical signal was collected by Helios software (Ultrafast Systems), and the data were processed by Surface Xplorer (Ultrafast Systems), where

background was subtracted and the chirp corrected.

The nanosecond transient absorption spectroscopy was collected with EOS spectrometer (Ultrafast Systems LLC) with the same pump pulse set up as the femtosecond experiment without using the chopper. The 2000 Hz probe pulse was generated by STM-2-UV (Leukos). The signals were processed by the same optical instrument and software as the femtosecond setup. Data were processed to generate transient absorption spectra, kinetic graphs, and triplet lifetime fitting by Igor Pro, WaveMetrics.

To acquire information about the singlet lifetime, time-corrected single photon counting (TCSPC) was applied to measure the fluorescence lifetime for BDP-TEMPO-S and BDP-TEMPO-L. The method followed the general setup in our lab[21]. To be specific, a model locked Ti:Sapphire laser (Millennia Pro, Spectra-Physics) generated femtosecond laser pulse of about 100 fs with a repetition rate of 80 MHz, and a pump pulse at 400 nm was generated by a BBO crystal from the fundamental 800 nm output. A pulse picker with 7 counts was applied, and the emission at 520 nm was selected by a monochromter and detected by a microchannel-plate-photomultiplier tube (Hamamatsu R3809U-51).

2.2 Results and Discussion

2.2.1 Synthesis and Characterization

The structure of BODIPY-N3 was characterized by ^{1}H NMR (400MHz INOVA) (Figure 5).

Note that although the molecular structure is presented as symmetrical in the planer drawing, the meso position azide is stereo hindered by the methyl groups on the BODIPY skeleton. Thus, the long range coupling created by the spatial effect makes the hydrogens on the BODIPY skeleton nonsymmetrical.
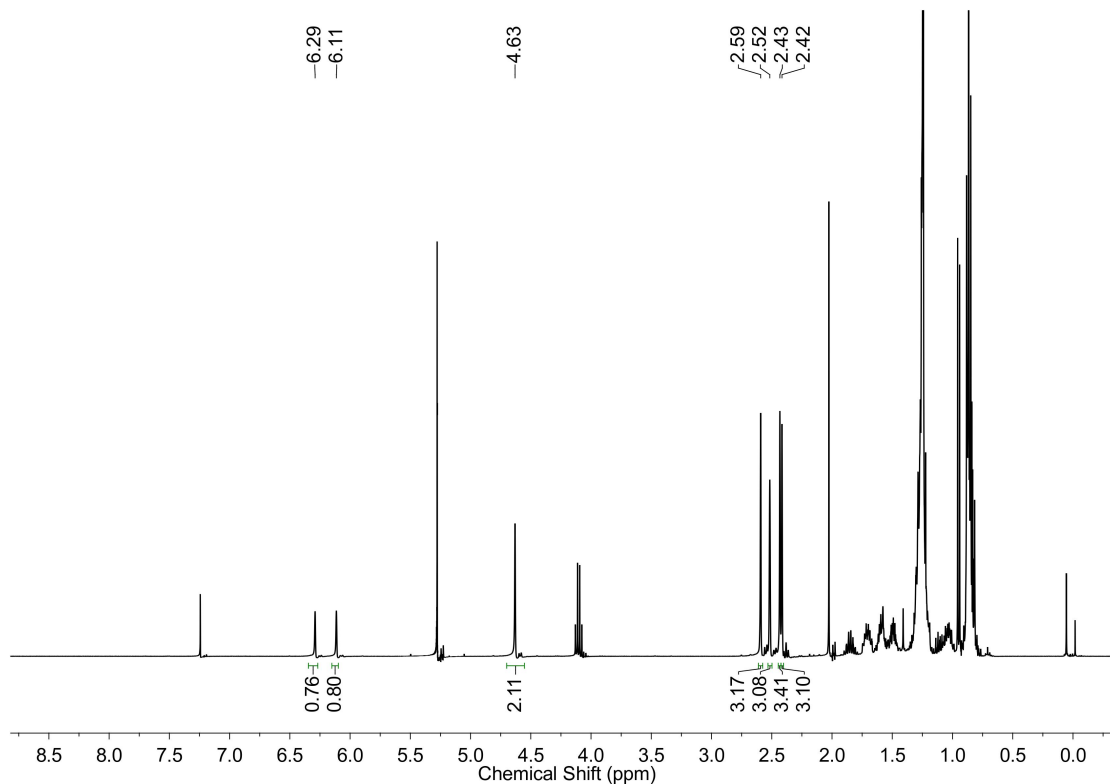
Figure 5: The ^{1}H NMR spectrum for BDP-N3.

Compounds **5** and **6** are characterized by ^{1}H NMR spectra obtained on a Bruker 500 spectrometer operated at 500 MHz at room temperature (Figure 6 and Figure 7), and the two BDP-TEMPO molecules were characterized by mass spectrometry. BDP-TEMPO-L has an experimental mass of 598.4052, which is close to the calculated mass as 598.5908. BDP-TEMPO-S has an experimental mass of 527.3835, while the calculated mass is 527.3889.

For BDP-TEMPO-M, the mass spectrometry pattern predicted by ChemDraw has a major peak of 513.296(100%) with two side peaks 512.299(24%) and 514.299(18%), which is consistent with the experimental result as shown in Figure 8.
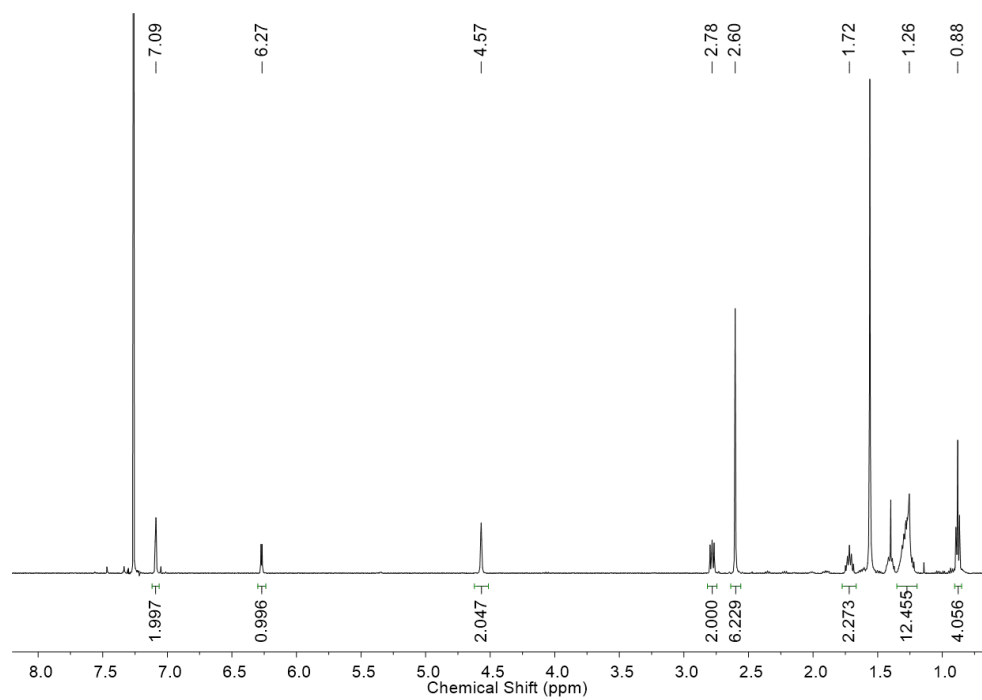
Figure 6: ^{1}H NMR spectrum of compound **5**
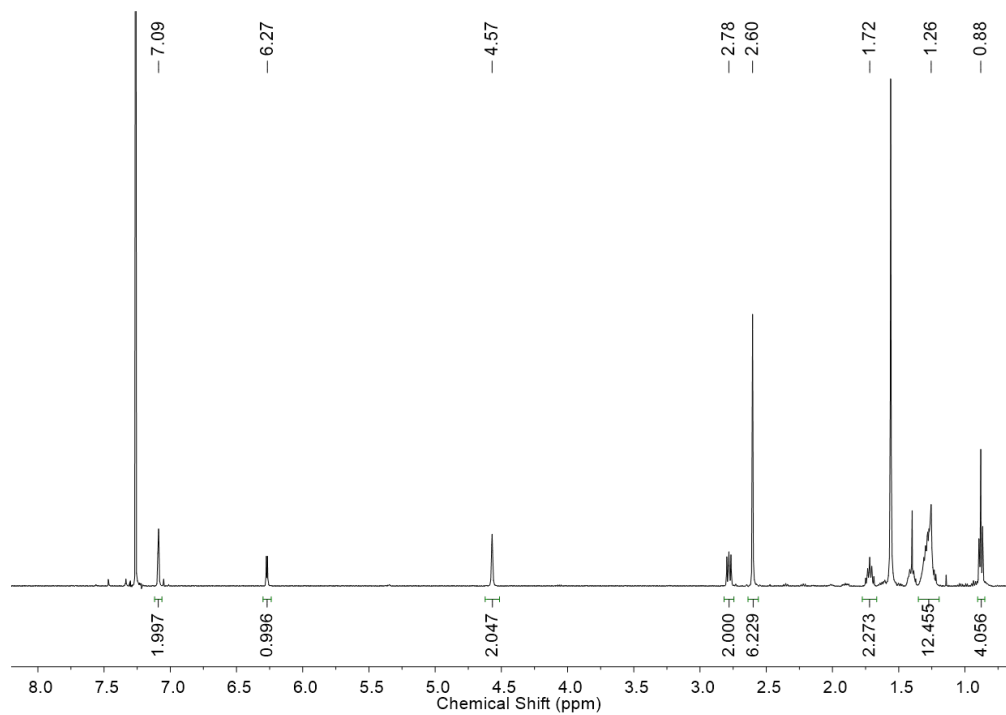
Figure 7: ^{1}H NMR spectrum of compound **6**
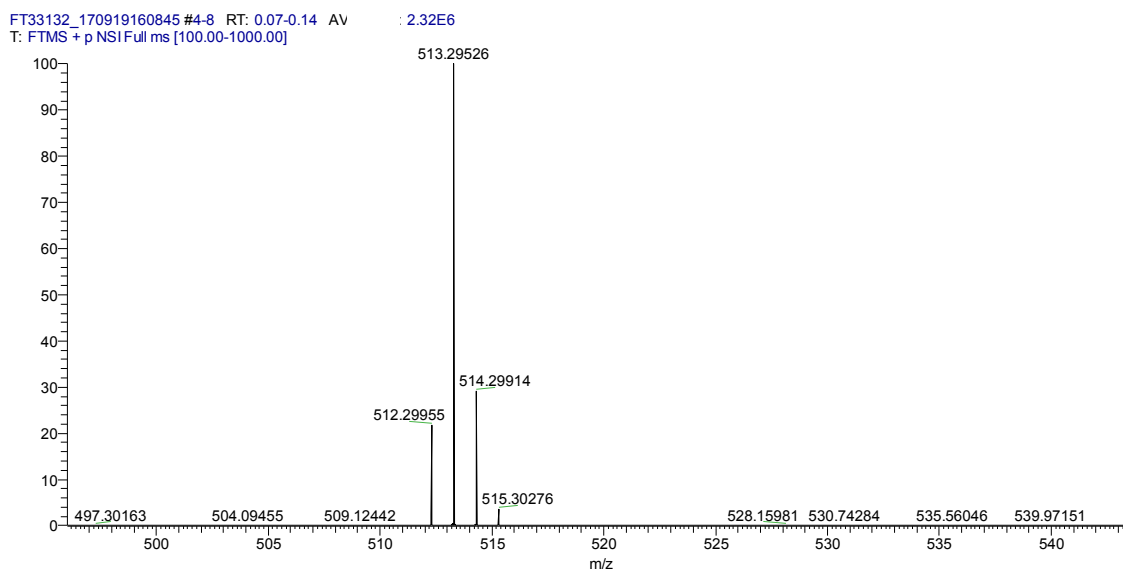
Figure 8: The mass spectrum of BDP-TEMPO-M

2.2.2 Steady State Analysis

The UV-Vis absorption spectrum and the fluorescence emission spectrum of BDP-N3 and BDP-TEMPO-M with the same concentrations are shown below (Figure 9). The attachment of a TEMPO radical did not shift the UV-Vis absorption pattern. The fluorescence emission, however, decreased a large amount, indicating a fluorescence quenching after the connection with TEMPO radical. This indicates the radical interferes with the singlet excited state to singlet ground state transition.
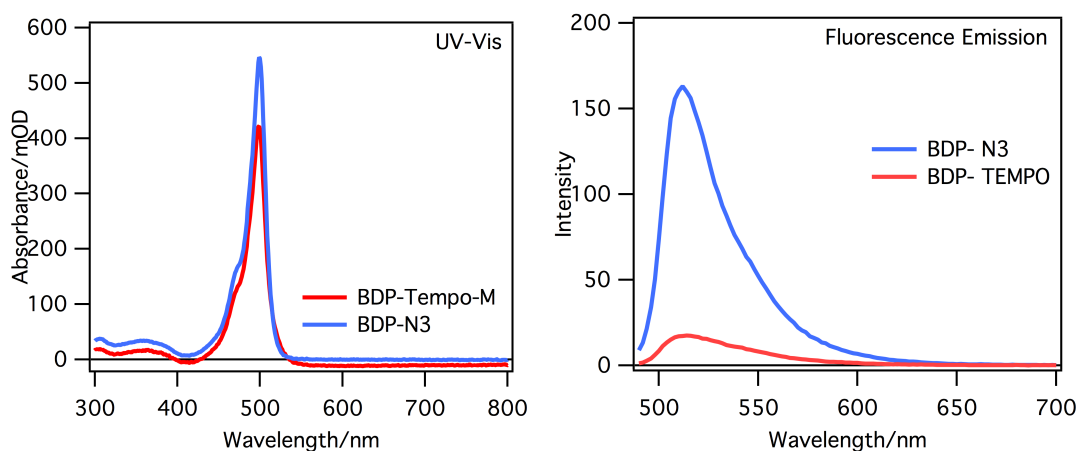
Figure 9: The UV-Vis (left) and fluorescence emission spectrum (right) of BDP-N3 and BDP-M

For BDP-TEMPO-S and BDP-TEMPO-L, the UV-Vis absorption spectra are shown as Figure 10. However, the fluorescence intensity appeared to be stronger than for BDP-TEMPO-M. The fluorescence spectra are shown below in Figure 11. The fluorescence intensity was plotted against the absorption values at 430nm with linear fit (Figure 12), and the fluorescence quantum yield calculated are shown in Table 1. The fluorescence quantum yield of BDP-TEMPO-L was slightly smaller than the BDP-TEMPO-S. This data can be compared to the calculated

fluorescence quantum yield from the excited state fitting analysis as a reference to verify the

accuracy and validity of the fitting.
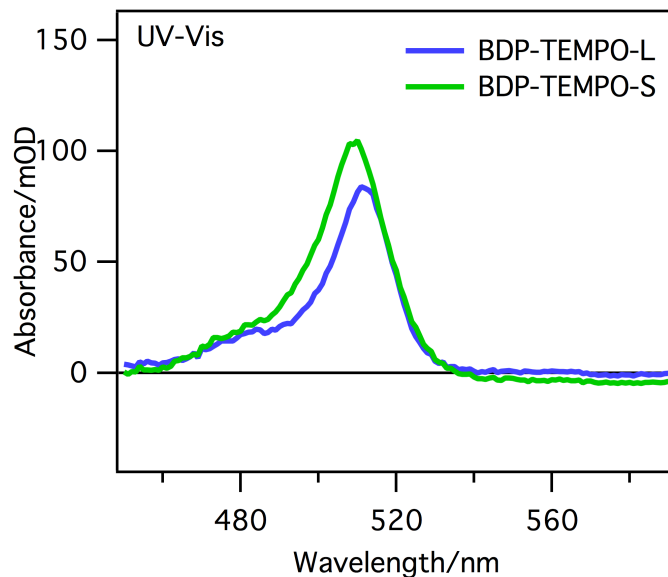
Figure 10: The UV-Vis absorption spectra of BDP-TEMPO-L and BDP-TEMPO-S after baseline

subtraction
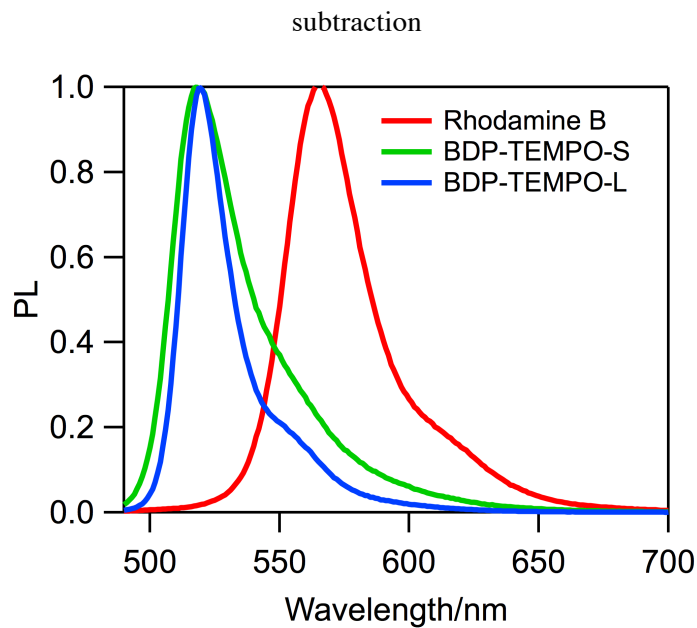
Figure 11: The fluorescence emission spectrum of BDP-TEMPO-S, BDP-TEMPO-L, and

Rhodamine B (as standard).
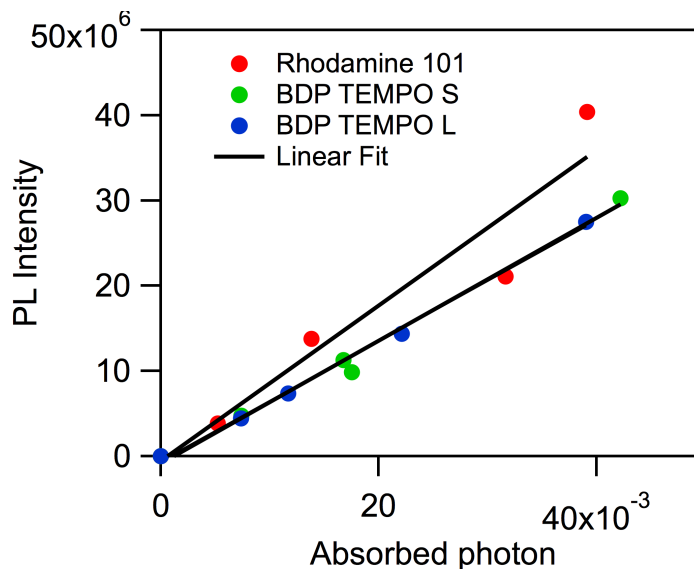
Figure 12: The linear fit of absorbance versus fluorescence intensity for fluorescence quantum

yield calculation.

Table 1: Fluorescence Quantum Yield Results

BDP-TEMPO-S	78.90%
BDP-TEMPO-L	77.60%

2.2.3 Excited State Analysis

Transient absorption spectra of BDP-N3 (Figure 13) showed ground state bleach at 400-420

nm, and an excited state absorption at 350-380 nm. Note that the sharp peak at around 403nm was

from the excitation pulse. The nanosecond scaled data shows the signal at around 50-100 ns had

decayed to the baseline, and the signal around 350-380 nm decayed completely at around 10-20

ns. This trend indicates that the peak centered at 360 nm was generated from singlet.

BDP-TEMPO-M had a similar spectrum, yet the trace at 1-2 μs still demonstrated a signal of decent intensity at the ground state bleach and excited state absorption part (Figure 13). This trend showed that the singlet and triplet state had signals at the same wavelength and the spectrum signals overlap. Thus, it is difficult to isolate out the singlet or triplet kinetic signals and apply the kinetic data to fitting for intersystem crossing rate (Figure 14). The triplet lifetime of BDP-TEMPO-M was determined via a relatively simpler approximate fitting at the ground state bleach wavelength 510 nm.

$$[A](t) = a_1 e^{-t/\tau_1} + a_2 e^{-t/\tau_2}$$

Singlet decay and intersystem crossing is convoluted into τ_1; here τ_2 represents the triplet lifetime.

The triplet lifetime was calculated as 2.12 μs (Table 2), which is notably different from the triplet lifetime reported by the literature[3]. Although this sample was prepared via the freeze-pump-solve method to ensure the oxygen free solvent environment, we still suspected that the sample was not sufficiently air tight and leaked oxygen, which as a ground state triplet, quenched the triplet of the BDP-TEMPO-M. Thus, the sample was prepared again in the glove box with an oxygen content of 15.5 ppm to confirm if the previous experiment was oxygen free, and the result was positive. The discrepancy of this experiment and the result reported by Wang[3] may be due to the difference in the power of the excitation pulses applied in the two experiments.
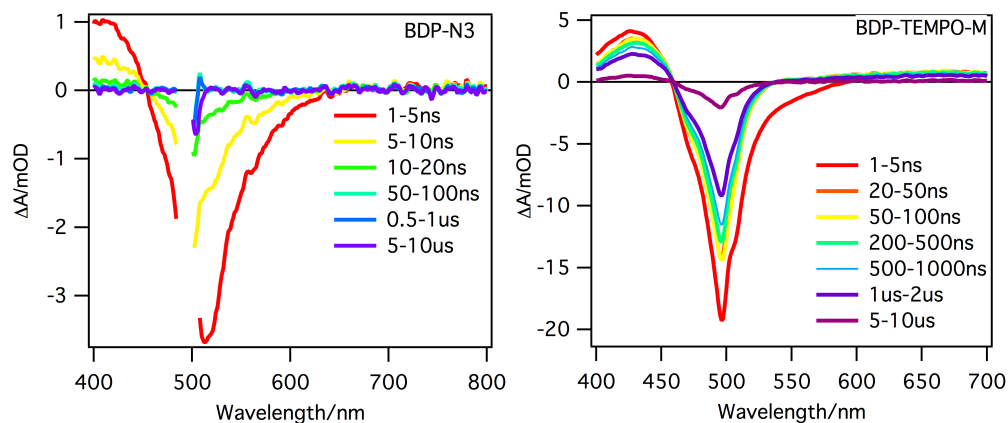
Figure 13: The transient absorption spectra for BDP-N3 (left) and BDP-TEMPO-M (right).
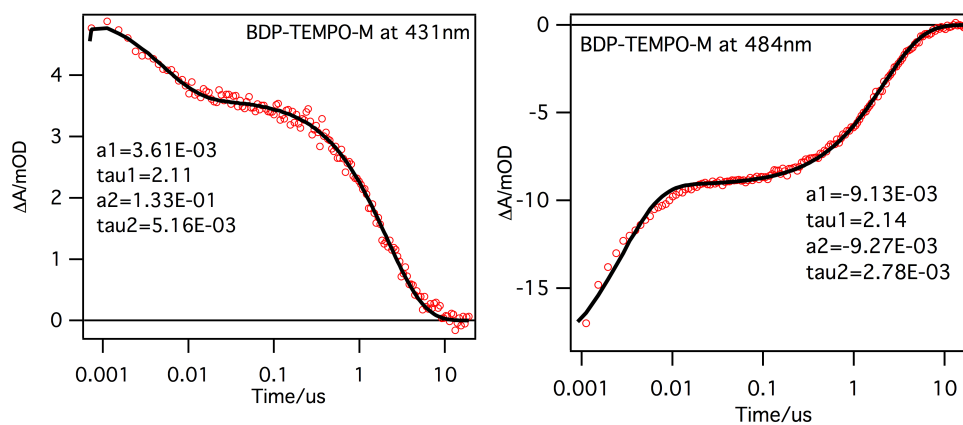
Figure 14: Kinetics for BDP-TEMPO-M, and fitting for assessment of the triplet lifetime

Table 2: Triplet and Singlet Lifetime Fitting Parameters

	τ_t	τ_s	Sample Prep
BDP-Tempo-M	2.12us	~4ns	Free pump solve, rt
BDP-Tempo-M Retest	1.09us	~3.8ns	Glove box, rt
BDP-N3	-	4.8ns	Glove box, rt
Lit[3]. BDP-Tempo	62us	0.2ns	Deaerated toluene, 20°C
Lit[3]. BDP-N3	-	5.7ns	Deaerated toluene, 20°C

The transient spectroscopy experiment for BDP-TEMPO-S and BDP-TEMPO-L presented a

larger wavelength range (Figure 15 and Figure 16), which demonstrates the triplet generation more obviously. To identify the singlet and triplet peaks, the spectra of 1-2 ps and 1.2-1.6 ns were isolated and normalized at the ground state bleach peak (Figure 17). By comparing these two spectra, two wavelengths were noticeable: 355 nm was ideal for singlet signal and 430 nm was ideal for triplet signal even though there was contribution from singlet signal. To be specific, the signal at 355 nm decayed completely in 1.2-1.6 ns, indicating that only singlet excited state absorption contributed to the signal. At around 430 nm, a broad signal was generated, maximized at 1.2-1.6 ns, and remained for tenth of microseconds. This long lasting signal represents the triplet state, and the initial signal at this wavelength indicates that 430 nm is a combination of the triplet and singlet signals. The spectra for BDP-TEMPO-S and BDP-TEMPO-L have a similar pattern and attribution with slight difference in the spectral shape and time scale possibly due to slightly different electronic structures introduced by different geometric structures. The triplet signal at 430 nm of BDP-TEMPO-S decays faster than BDP-TEMPO-L (Figure 15 and Figure 16).
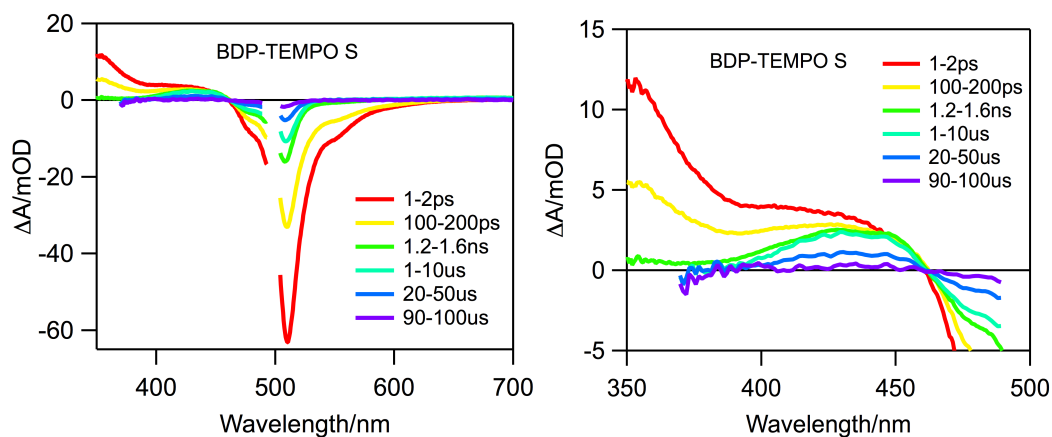
Figure 15: Transient absorption spectra for BDP-TEMPO-S with larger view on 355-480 nm

region for identifying singlet and triplet.
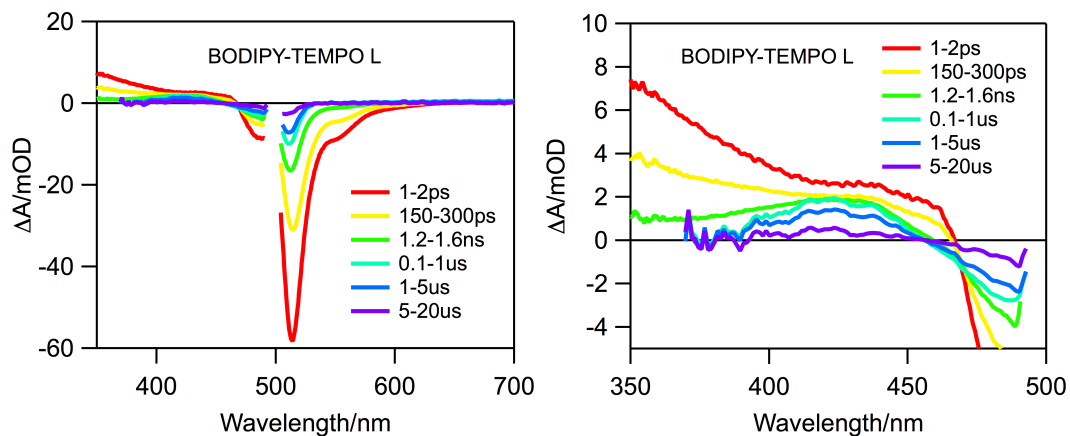
Figure 16: Transient absorption spectra for BDP-TEMPO-L with larger view on 355-480 nm

region for identifying singlet and triplet.
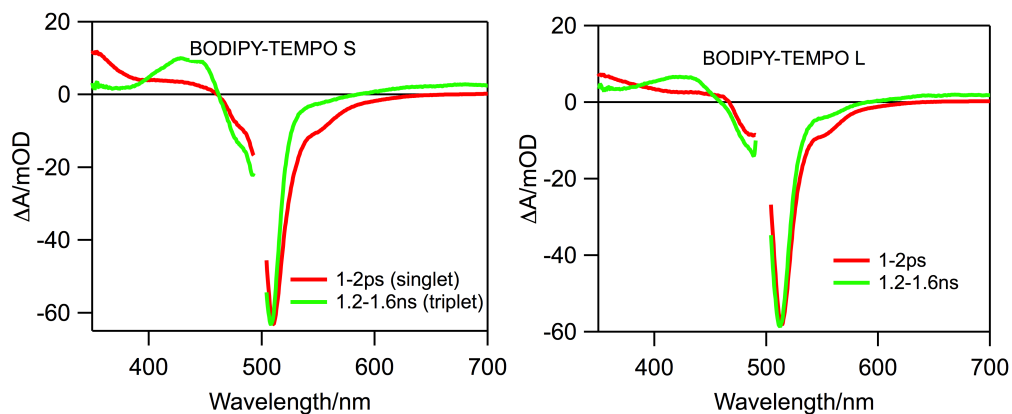
Figure 17: Singlet and triplet spectra of BDP-TEMPO-S and BDP-TEMPO-L.

With the singlet and triplet signals identified, the kinetics at 355 nm was plotted as the pure

singlet kinetics. Related rate constants were obtained from fitting of the kinetics at different

wavelengths. As demonstrated in Figure 18, three decay processes were present for the

BODIPY-TEMPO molecules after excitation. First, singlet excited state (BDP_S^*) could decay by

either intersystem crossing (k_{isc}) or directly returning to the ground state (k_{SD}) through either

radiative fluorescence decay or non-radiative internal conversion coupled to vibration. The triplet

excited state (BDP_T^*), which is the ISC product, is only able to decay through another intersystem

crossing process to the ground state (k_{TD}).
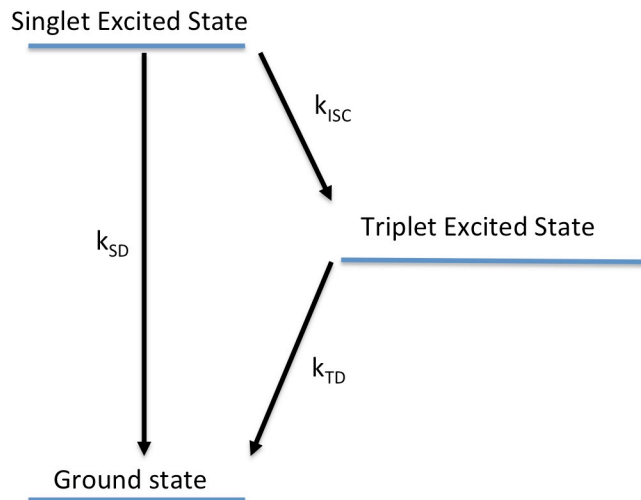
Figure 18: Illustration of the possible decay pathways for the singlet excited state.

Following this model, the expression for the singlet excited state kinetics is shown below.

$$[BDP]_S^*(t) = [BDP]_S^*(0)e^{-(k_{SD}+k_{isc})t} \qquad \text{Eq S1}$$

The triplet excited state population growth and decay can be expressed as:

$$\frac{d[BDP]_T^*(t)}{dt} = k_{isc}[BDP]_S^*(t) - k_{TD}[BDP]_T^*(t) \qquad \text{Eq S2}$$

Integrating and solving EqS2 provides the triplet excited state kinetics as:

$$[BDP]_T^*(t) = \frac{[BDP]_S^*(0)k_{isc}}{k_{SD}+k_{isc}-k_{TD}}[e^{-k_{TD}t} - e^{-(k_{SD}+k_{isc})t}] \qquad \text{Eq S3}$$

The kinetics data of three wavelengths identified above were used to extract the singlet and triplet

excited states, and a global fitting was done since clean triplet signals were not available in the

350-900 nm range. First, the ground state bleach peak at 509 nm, contributed by both singlet and

triplet excited state, had kinetics defined by:

$$\Delta A(509nm) = -\varepsilon_{BDP}(509nm)\left[[BDP]_S^*(t) + [BDP]_T^*(t)\right] \quad \text{Eq S4}$$

Here, $\varepsilon_{BDP}(509nm)$ is the extinction coefficient of ground state at 509 nm obtained from steady

state UV-Vis absorption spectrum. The second wavelength chosen is at 430 nm, which has an

identifiable triplet excited state absorption as discussed above. Since this wavelength also has a

contribution from singlet excited state absorption at early time, the expression is written as:

$$\Delta A(430nm) = \varepsilon_S(430nm)[BDP]_S^*(t) + \varepsilon_T(430nm)[BDP]_T^*(t) \qquad \text{Eq S5}$$

Here, $\varepsilon_S(430nm)$ and $\varepsilon_T(430nm)$ is the extinction coefficient of singlet and triplet excited

state absorption at 430 nm respectively. The $\varepsilon_T(430nm)$ is pre-determined by the ratio of the

signal amplitude at 430 nm and 509 nm at 1.2-1.6 ns. Similarly, the $\varepsilon_S(430nm)$ is

predetermined by the relative ratio of the signals at 430 to 509 at 1-2 ps. In this time range, the

singlet excited state decayed away. The third wavelength, 355 nm, is identified as a clean singlet

ESA and represented as:

$$\Delta A(355nm) = \varepsilon_S(355nm)[BDP]_S^*(t) \quad \text{Eq S6}$$

Here Eq. S1 and Eq. S2 is substituted into Eq. S4 to S6, the kinetics could be fitted using these
two equations globally. The global fitting curve is shown in Figure 19 and Figure 20. The fitting
parameters are summarized in

Table 3.
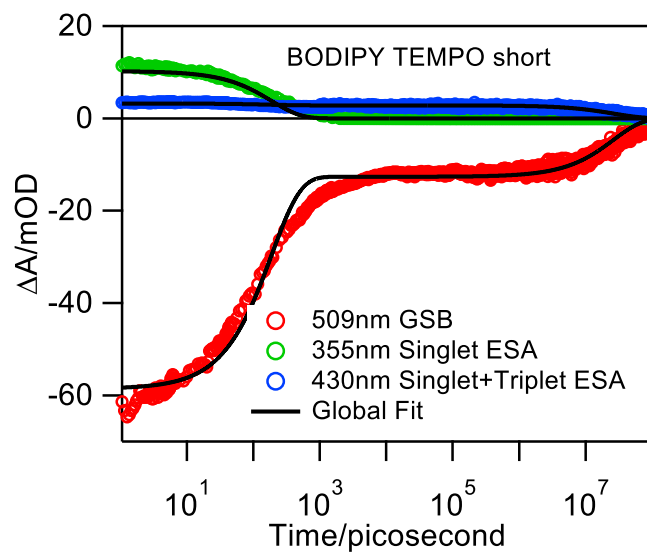
Figure 19: Ground state bleach kinetics, 355nm pure singlet kinetics, and 430nm singlet triplet

kinetics, and global fitting curve of BDP-TEMPO-S
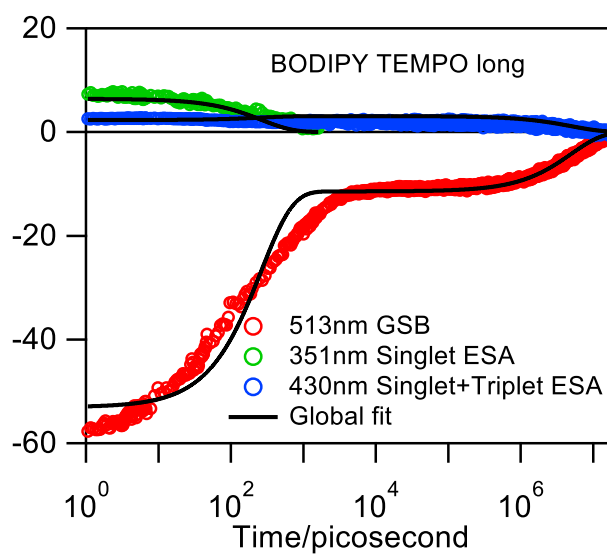
Figure 20: The kinetics and fitting curves of related wavelength to determine rates for

BDP-TEMPO-L.

Table 3: Fitting Parameters for BDP-TEMPO-S and BDP-TEMPO-L

		BDP-TEMPO-S		BDP-TEMPO-L
Extinction	509nm	1.03×10^5	513nm	7.17×10^4
	355nm	S 1.798×10^4	351nm	S 8.65×10^3
	430nm	S 0.564×10^4	430nm	S 3.11×10^3
	430nm	T 2.281×10^4	430nm	T 1.92×10^4
rate	S to G	$4.14\times10^{-3}\pm4.88\times10^{-5}$		$2.97\times10^{-3}\pm5.65\times10^{-5}$
	isc	$1.14\times10^{-3}\pm1.40\times10^{-5}$		$8.20\times10^{-4}\pm1.65\times10^{-5}$
	T to G	$3.79\times10^{-8}\pm6.90\times10^{-9}$		$2.00\times10^{-7}\pm1.59\times10^{-8}$

To verify the fitting parameter, the fluorescence quantum yield was applied as a reference. Since the ISC process contributed to the loss in fluorescence quantum yield, the ratio of singlet to ground state transition rate versus total rate for singlet excited state extinction was the same as or smaller than the florescence quantum yield (Table 1), which indicated the validity of the fitting.

As shown above, the intersystem crossing rate of BDP-TEMPO-S was higher than BDP-TEMPO-L while the triplet decay rate of BDP-TEMPO-S was smaller, which means the triplet lifetime for BDP-TEMPO-S is longer. This finding is different from those in many literature studies[3, 12] which report the intersystem crossing rate is directly related to the length of the linker between radical and organic chromophore, and the triplet lifetime inversely correlates with the distance. In the reported literature, the intersystem crossing rate correlates somewhat with the triplet decay rate in the sense that both processes are spin forbidden and are facilitated by

the radical assisted spin flip. This difference may be caused by the unique molecular structure of BDP-TEMPO-S, in which the TEMPO radical is one covalent bond away from the BODIPY unit. This shortest possible linkage creates a rigid structure that does not allow the radical to rotate or flip over and spatially approach the chromophore. On the other hand, the distance dependence experiments done by Wang et al[3] investigated BODIPY-TEMPO molecules with six and eleven covalent bond linkers, both long and flexible enough to create spatially affinity. Several interpretations can be made regarding this finding. First, the result of our experiment supports the through-bond influence of the distance effect of radical EISC since BDP-TEMPO-S demonstrated a high EISC with little spatial radical-chromophore interaction. Second, the triplet to ground state transition may be related to the spatial interaction, which explains the long lifetime of BDP-TEMPO-S. Nevertheless, BDP-TEMPO-S demonstrates a possible structure in which the ISC rate and triplet state lifetime can be enhanced simultaneously, which is a desirable feature for radical EISC in organic chromophores and for future applications.

2.3 Conclusion

In summary, the BODIPY-TEMPO system exhibits radical EISC, and that the EISC effect is distance and position dependent. BODIPY-N3 without modification has very limited triplet quantum yield of less than 1%. Attaching the TEMPO radical on the meso position increased the ISC rate to a detectable range, yet the experimental triplet lifetime, measured as ~2μs, is shorter than previously reported. BDP-TEMPO-S and BDP-TEMPO-L exhibit a distance

dependence of radical EISC.

This is the first time that the distance dependence of radical EISC exhibits a direct relationship between the ISC rate and the triplet lifetime, a features that may be due to the rigid structure of BDP-TEMPO-S. Since a high ISC rate and a long triplet lifetime are both desirable features of radical EISC, we believe that our findings in these chromophore-radical systems with both properties will contribute to the development of organic radical photosensitizers. There will be simulation study follow-ups to address the fundamental reason(s) for the impact of structure on the spin forbidden processes.

Chapter 3. Anthracene System

3.1 Methods

3.1.1 Synthesis

The starting materials, solvents, and catalysts were purchased from OCI Chemical Company (anthracene carboxylic acid), and Sigma-Aldrich Chemical Company (all other materials). Anthracene with TEMPO attached at position 9 (ACA-TEMPO), and anthracene-9,10-dithiol (ACA-SH) were synthesized from 9-anthracenecarboxylic acid (ACA). The synthetic process for ACA-TEMPO was performed following the literature procedure[22], while some adjustments were made after examining the results of the unsuccessful trials. To synthesize ACA-SH, 3g of ACA was added into a 50 ml flame-dried, round bottom flask, and 15 ml thionyl chloride was added and well stirred at 80 °C under reflux overnight. The remaining thionyl chloride was removed by distillation at 100 °C, followed by high vacuum for 2 hours. Note that the solvent trap of the vacuum was placed in liquid nitrogen, and the removed thionyl chloride was quenched with saturated KOH solution. The reaction mixture was examined with thin layer chromatography (TLC) and the product had an Rf value of 0.9 in 20% ethyl acetate in hexane. After removing thionyl chloride, the reaction mixture appeared to be brown, and was diluted in 100 ml of methylene chloride. The solution was washed with brine, dried over Na_2SO_3 and then concentrated by evaporation under reduced pressure. The compound was purified by column

chromatography on silica gel with 10:90 ethyl acetate to hexane. The product appeared to be a yellow-orange oil, and the structure was confirmed by ^{1}H NMR, IR, and mass spectrometry. The yield of this reaction was very low, since this reaction was intended to make the acid chloride.

For ACA-TEMPO synthesis, 1g of ACA was added into a 50 ml flame-dried, round bottom flask, and 10 ml thionyl chloride was added and well stirred at 80 °C under reflux overnight. Excess thionyl chloride was removed by distillation at 100 °C, followed by high vacuum for 2 hours. An NMR spectrum was taken to ensure the major compound in the reaction mixture was anthracene 9-acid chloride. Then, 170 mg of the reaction mixture was placed in another flame-dried 50 ml round bottom flask, and diluted with 4 ml methylene chloride. Another solution was prepared with 150 mg 4-amino TEMPO in 4 ml of methylene chloride, and this was added to the stirred anthracene acid chloride solution. White smoke was generated during the addition. Then, 0.3 ml of triethylamine was added into the solution which was then stirred at 35 °C for 2 days.

All compounds were confirmed by ^{1}H NMR spectroscopy in $CDCl_3$ solution, infrared Spectroscopy (IR) (Nicolet iS10, Thermo Scientific), UV-Vis, and mass spectrometry.

3.1.2 Steady State Absorbance and Fluorescence

UV-Vis absorption spectra for ACA-SH were measured by the same instrument for both BDP-TEMPO-L and BDP_TEMPO-S. The steady state fluorescence emission spectra were measured by Fluoromax 3 with an excitation pulse of 350 nm. Samples were dissolved in toluene with a concentration of 10^{-5}M, and the solutions were prepared under air at room temperature.

Spectra data were processed by Igor Pro, WaveMetrics. Fluorescence quantum yield was measured and calculated with the same method and instruments as described in section 2.1.2.

3.1.3 Excited State Transient Spectroscopy

The femtosecond and nanosecond transient absorption experiments were performed with the same setup as used for BODIPY measurements explained in section 2.1.3 with slight modifications. The pump light was adjusted to 400 nm for ACA-TEMPO and ACA-SH, and the 400 nm pulse was generated by doubling the fundamental 800 nm beam.

3.2 Results

3.2.1 Synthesis

The synthesis for ACA-TEMPO was performed first, and a TLC product spot with an 0.9 Rf value was isolated. Since the product point showed blue fluorescence under UV light, and the UV-Vis absorption spectrum approximately fit the literature description[22], we assumed the compound isolated was ACA-TEMPO. However, when we replicated the experiment, we noticed the product point appeared on the TLC plate before TEMPO was even added to the reaction mixture. Thus, it is highly possible that the product did not have TEMPO in its structure. Then, we replicated the experiment without adding 4-amino-TEMPO as described in the method section and used more characterization techniques including ^{1}H NMR, carbon NMR, IR, and mass spectrometry.

The ^{1}H NMR result (Figure 22) only showed two equally integrated double doublet signals at 7.64 and 8.55 ppm, indicating that on the anthracene skeleton there were two chemically distinct hydrogens, and each signal showed two magnetically distinct hydrogens. From the CNMR spectrum (Figure 21), there are four signals in the aromatic region. The H-NRM and CNMR results agree with each other in that the main structure of the product is an anthracene disubstituted at the 9,10 positions, and the symmetry in the spectra indicates that the substituents on the 9, and 10 position are the same.

The IR did not show any significant peaks that indicated carbonyl or amide group (Figure 23).

To attempt to further characterize and thus clarify the product, a crystal structure of this molecule was obtained with a Rigaku Synergy-S diffractometer with a HYPIX detector (Figure 24). The crystal structure showed this molecule was an anthracene with sulfur molecule and a proton attached at the 9 and 10 position (ACA-SH), which is consistent with the NMR and IR results.
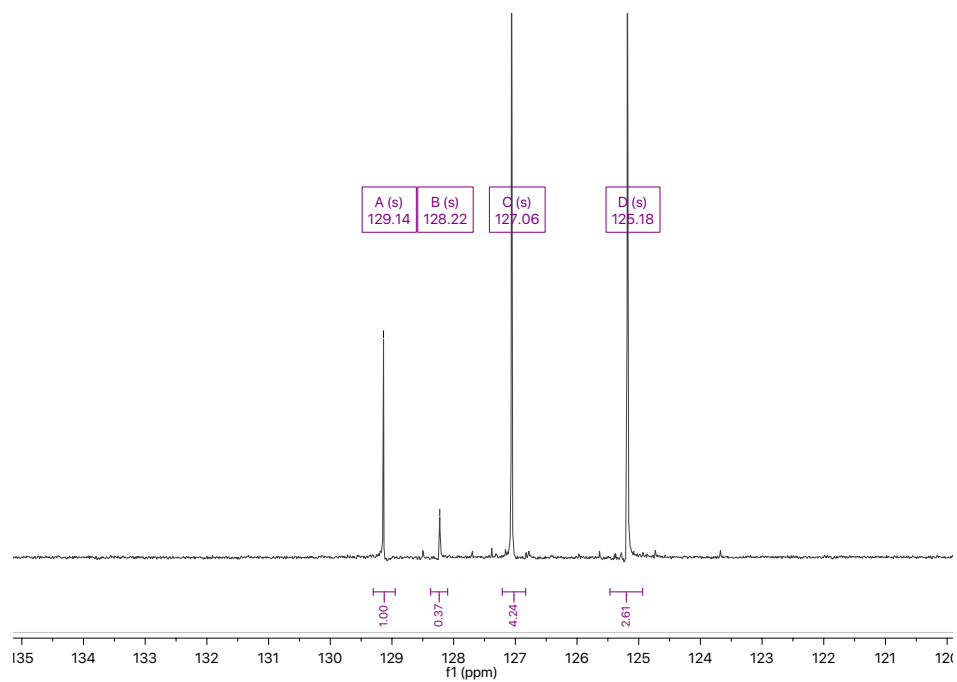
Figure 21: Carbon NMR spectrum for ACA-SH
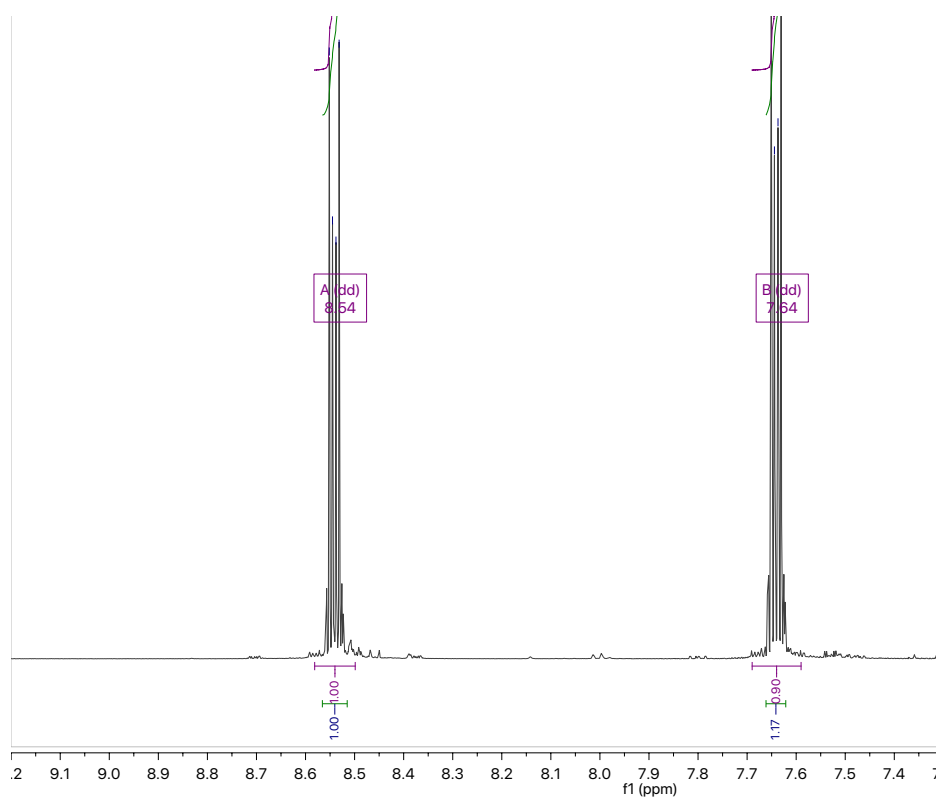
Figure 22: ^{1}H NMR spectrum for ACA-SH of the aromatic area signals.
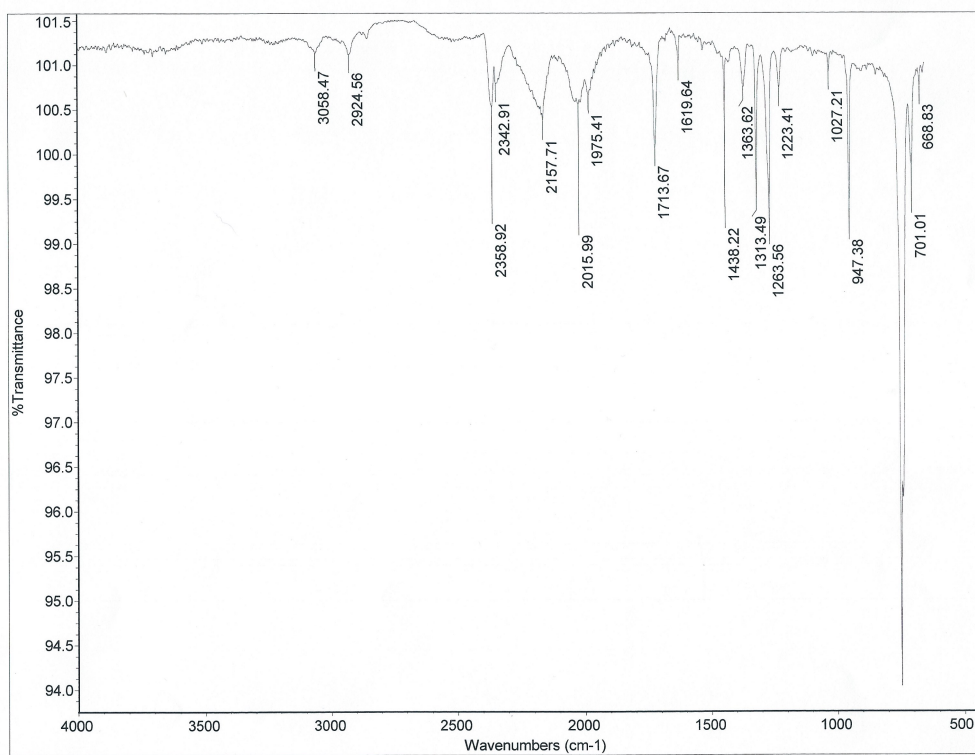
Figure 23: ACA-SH has no major peaks on IR spectrum.
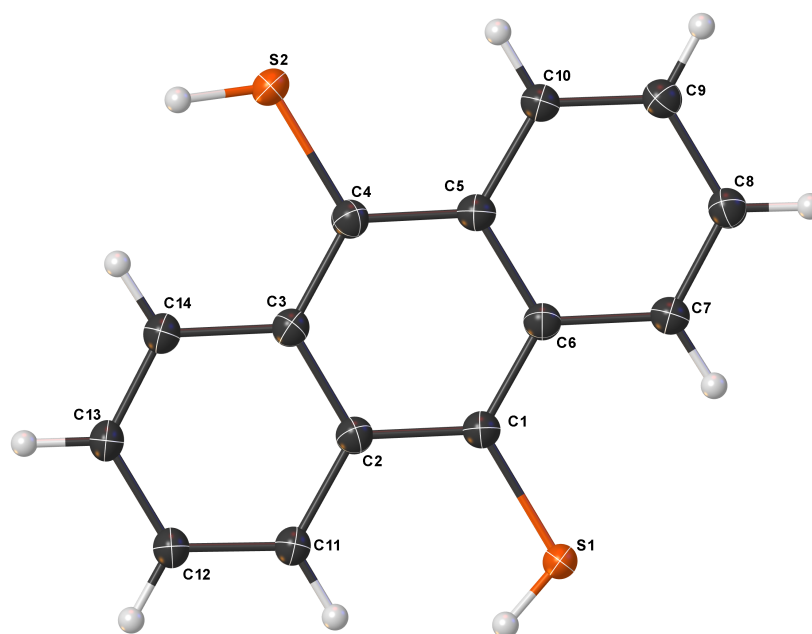
Figure 24: XRD crystal structure for ACA-SH

After confirming the identity of the ACA-SH sample, the ACA-TEMPO synthesis was

repeated, and a product spot with an Rf value of 0.2 in 10% methanol in methylene chloride was isolated. And the structure was characterized with ^{1}H NMR, IR, and mass spectrometry. Since a TEMPO radical has a free spinning electron that influences the magnetic spin, NMR was only able to detect the hydrogen signals on the aromatic system. The ^{1}H NMR spectrum (Figure 25) showed five signals with the most downfield peak integrated to one and the other four peaks integrated to two for each peak. This demonstrates a mono substituted anthracene at position 9.
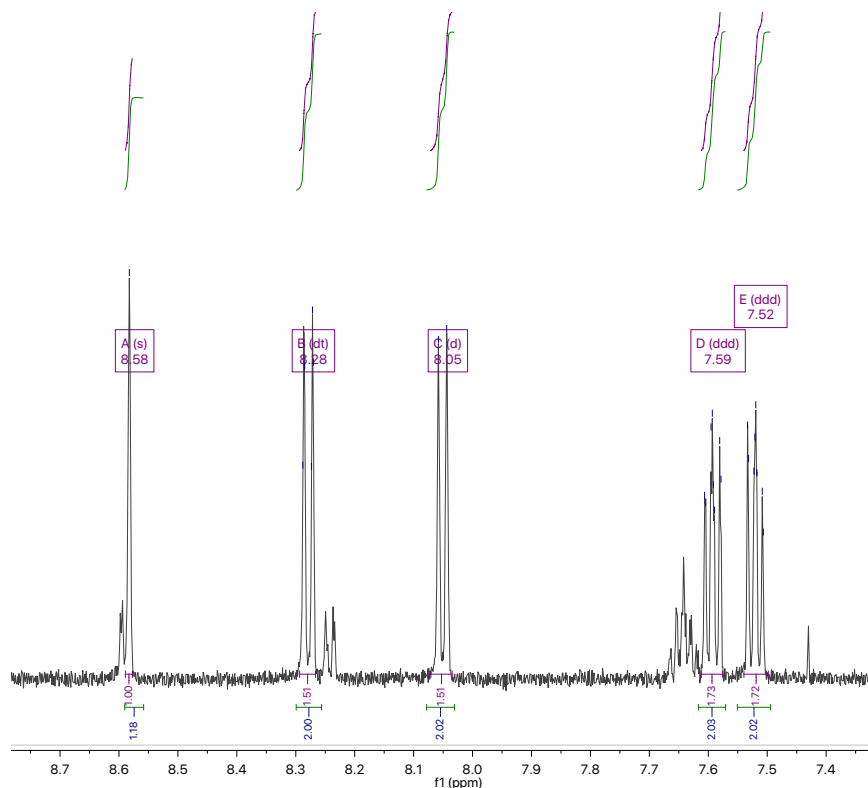
Figure 25: ^{1}H NMR for ACA-TEMPO only provides relatively reliable information in the aromatic region due to the radical influence.
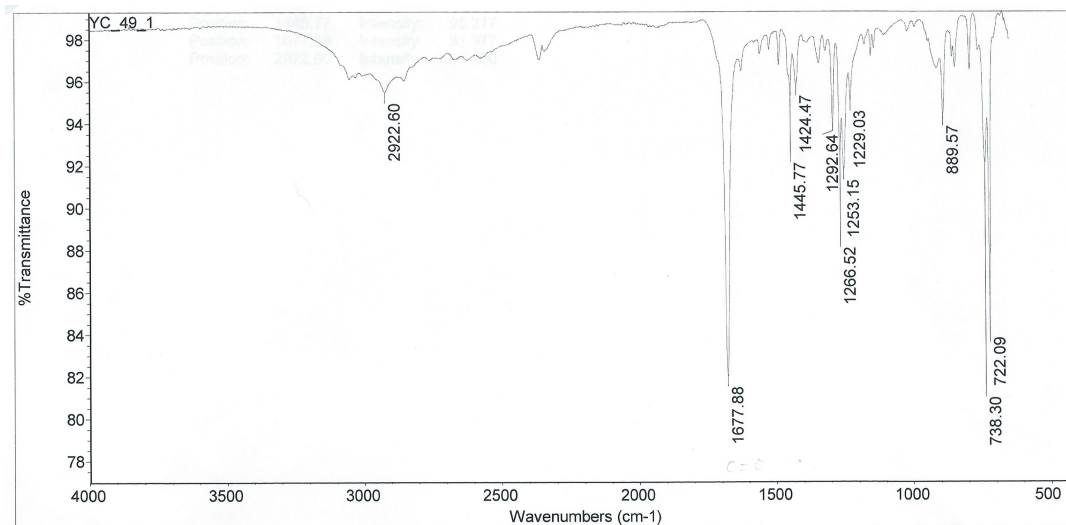
Figure 26: IR spectrum of ACA-TEMPO shows an amide C=O bond.

The IR spectrum (Figure 26) shows an intense peak at 1685cm^{-1}, indicating a C=O bond in an amide. This signal is very important because it demonstrates that the amine group on the TEMPO radical reacted with the acid chloride group on the anthracene, which strongly suggests the reaction was successful.

The liquid chromatography mass spectrometry (LCMS) (Figure 27) showed a major elution at 13.77 retention time with a mass value of 374.14, which matches with the calculated value of 374.19. The combined information from NMR, IR, and LCMS confirmed the structure of ACA-TEMPO molecule.
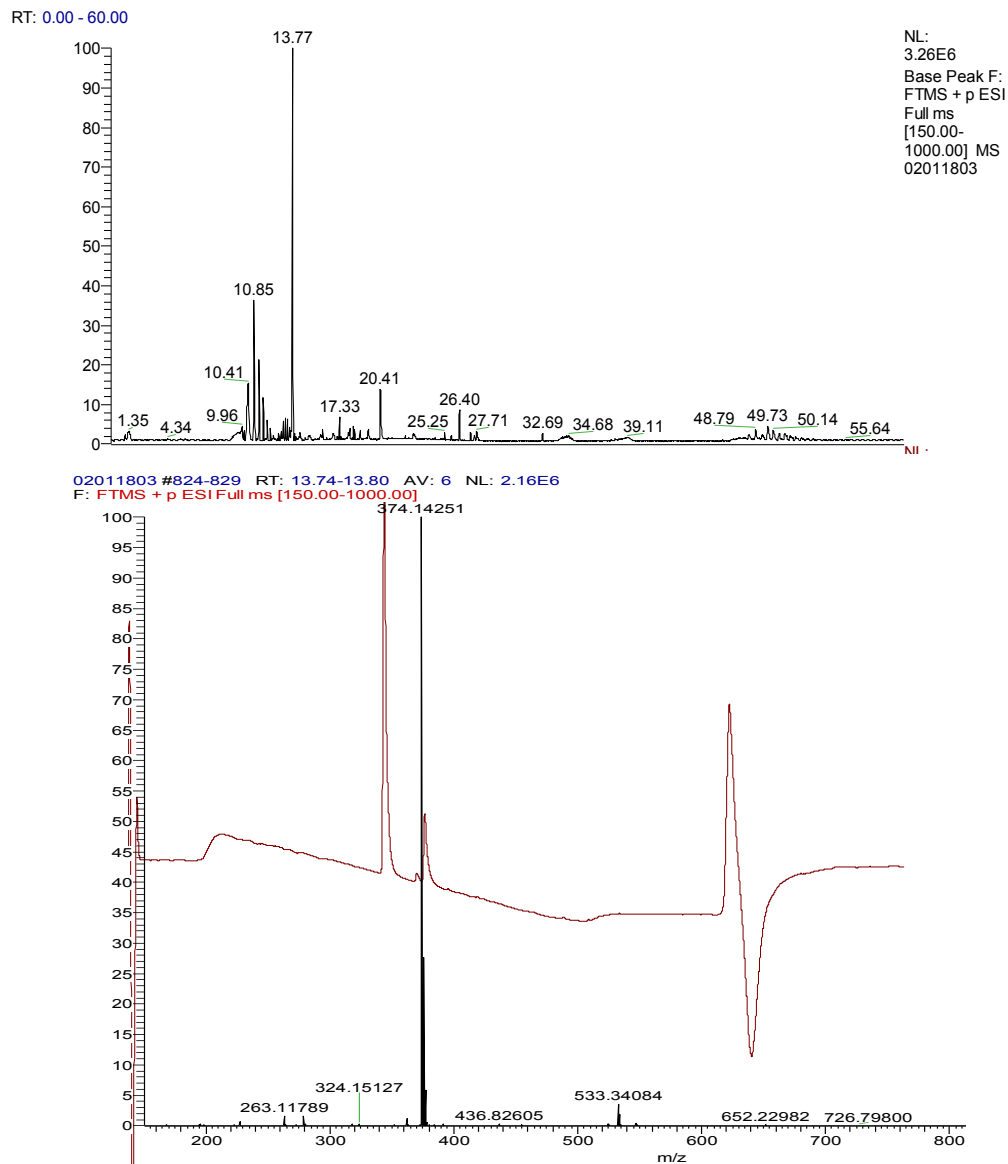
Figure 27: LC (top)-MS (Bottom) of ACA-TEMPO

3.2.2 Absorbance

The UV-Vis absorption spectrum and the fluorescence emission spectrum of ACA, ACA-SH and ACA-TEMPO with the same concentrations are shown below (Figure 28). The attachment of a TEMPO radical did not shift the UV-Vis absorption pattern, yet ACA-SH created a red shift in

the absorption peaks.
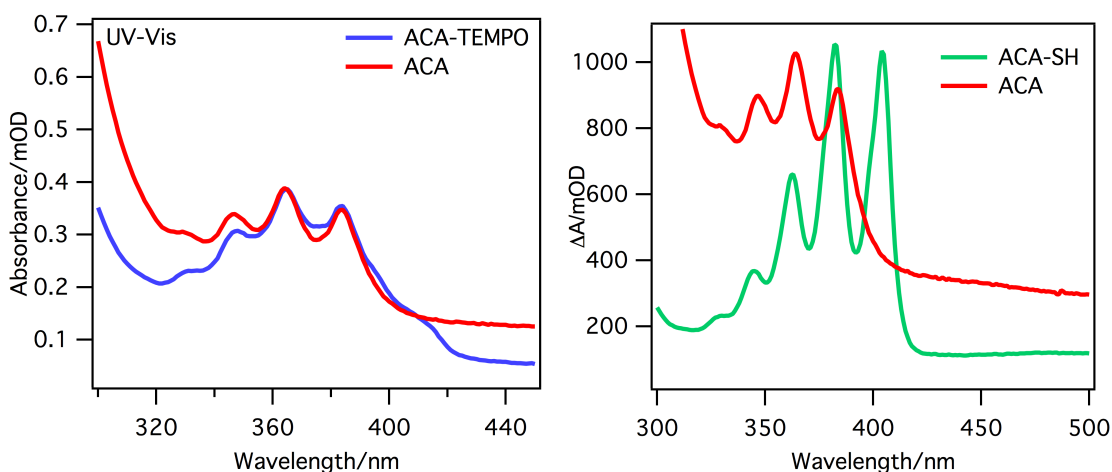
Figure 28: The UV-Vis absorption spectra of ACA, ACA-SH, and ACA-TEMPO

3.2.3 Excited State Study

Transient absorption spectroscopy of ACA, ACA-SH and ACA-TEMPO was done (Figure 29). This transient absorption data covers the wavelength range 380-730 nm, yet the ground state absorption of ACA is around 340 nm. Thus, the ground state bleach is not visible in the spectra, and all the signals are mostly excited state absorption. The broad peak at around 550-650 nm decays completely at around 50 ns, which is identified as the singlet decay signal. The triplet signal shows up at 430 nm, the small peak that grows and decays between 10 μs and 50 μs. In addition, assuming that adding a carboxylic group does not shift the triplet position, this triplet identification is also supported by literature[23]. In comparison to the ACA spectra, ACA-SH provides a distinct spectra shape and a clear increase in the excited state absorption at 430 nm. The 600 nm signal decays entirely at 50ns, which agrees with the ACA spectra and can be

identified as the singlet decay trace. The 430 nm signal increases from 10 ps to 1 ns, decreases for the 1.5 ns spectrum, and increases from 1-2 ns to 20 μs. This process describes a combination of singlet and triplet state. The pure triplet kinetics can be acquired by normalizing the 10-20 ps kinetics at 600 nm then subtracting from the 430 nm kinetics. With the acquired kinetic data, a global fitting can be done with the same fitting function as shown above in 2.2.3, which describes the rates for singlet decay, triplet decay, and intersystem crossing. The fitting parameter and the fitting spectra are shown below (Table 4 and Figure 30). Figure 31 more directly compares the triplet kinetics of ACA and ACA-SH.
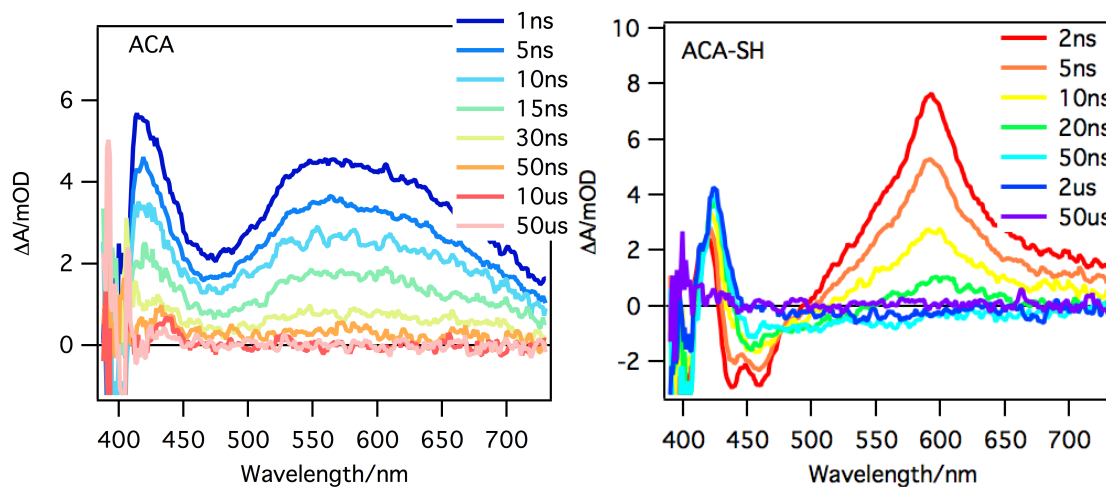
Figure 29: Traansient absorption spectra of ACA (left) and ACA-SH (right).
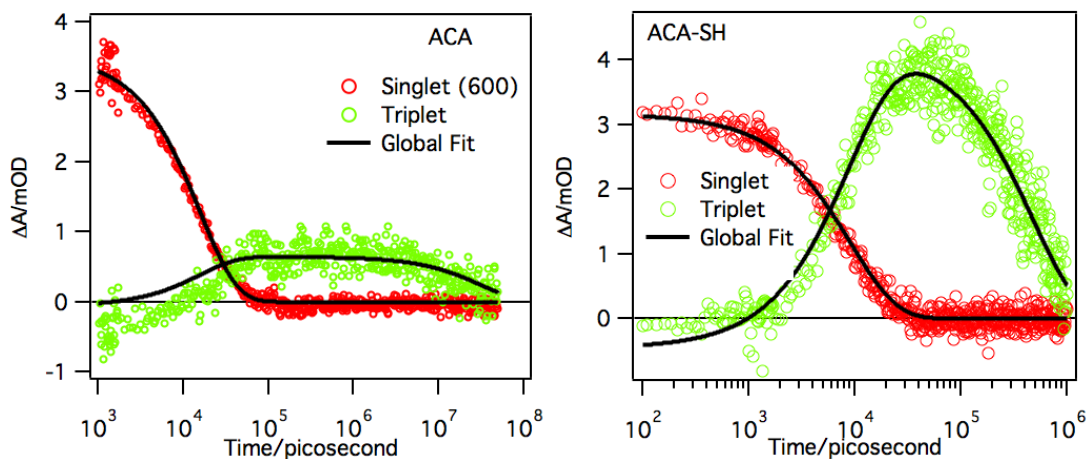
Figure 30: Singlet and triplet kinetics and global fitting for ACA(left) and ACA-SH(right)
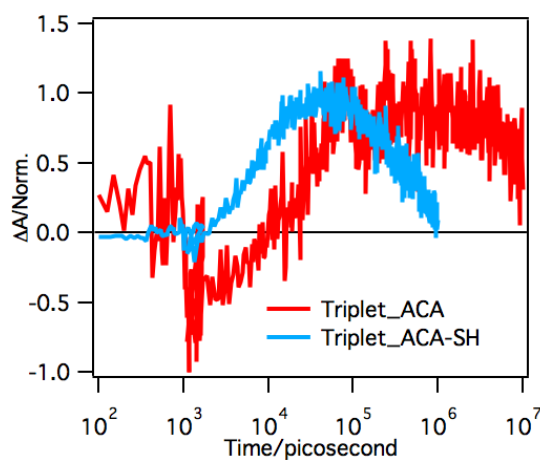
Figure 31: Direct comparison of the triplet kinetics of ACA and ACA-SH

Table 4: Fitting Parameters of ACA and ACA-SH

	Anthracene	Anthracene-SH
$k_{singlet}$	$5.41 \times 10^{-5} \pm 8.58 \times 10^{-5}$	$4.15 \times 10^{-5} \pm 3.07 \times 10^{-4}$
$k_{triplet}$	$3.16 \times 10^{-8} \pm 4.77 \times 10^{-8}$	$2.10 \times 10^{-5} \pm 5.37 \times 10^{-8}$
k_{isc}	$9.53 \times 10^{-6} \pm 8.55 \times 10^{-5}$	$6.4 \times 10^{-5} \pm 3.0 \times 10^{-4}$

The ISC rate (Table 4) of ACA-SH is higher than ACA, indicating that without a radical,

thiol groups are able to enhance ISC rate of ACA. One hypothesis is the sulfur atoms linked to ACA are slightly heavier than the carbon atoms. A heavier atom with a higher atomic number increases the rate of spin-orbit coupling. The spin-orbit coupling splits the original orbit into multiple orbits at different energy levels with different angular momentum quantum numbers and different spin quantum numbers, which increases the probability of achieving an allowed transition. This effect leads to an increased ISC rate. In addition, adding two thiol groups may slightly alter the structure of anthracene skeleton, facilitating EISC. Another hypothesis to explain this effect is that since sulfur is larger and less electronegative, the S-H bond is relatively weaker than O-H or C-H bonds, and the S-H bond may dissociate or partially dissociate more easily. As the S-H bond partially dissociates, the electrons between the two atoms may create a radical-like environment, which creates spin assisted EISC. In addition, adding two thiol groups may not change the electronic and energetic orbital of anthracene, which means this modification does not introduce other undesired competitive processes such as charge transfer. To further examine this hypothesis, the thiol group needs to be attached to different chromophores to verify the generality and applicability of this radical-like effect. Although further investigation is needed to understand the effect of thiol groups on ACA, the EISC of ACA-SH is significant since it not only has a high ISC rate compared to ACA, but also because it is more stable since it does not involve radicals. Thus, we believe that ACA-SH could be important in the future development and application of heavy-metal-atom-free triplet photosensitizers.

For the ACA-TEMPO molecule, the transient absorption data had the same problem that the

380-900 nm data did, which was the inability to include the ground state bleach signal (Figure 32).

The spectrum shape of ACA-TEMPO and 1-5 ns appeared similar to the spectra of ACA, yet the

shape diverged with time. It is difficult to identify the singlet and triplet decay wavelength since

the signal at all wavelength grows and decays in a similar time scale range, and no peak grows in

at a different time range. In the picosecond time scale, 820-880 nm shows a small signal that

decays extremely rapidly.
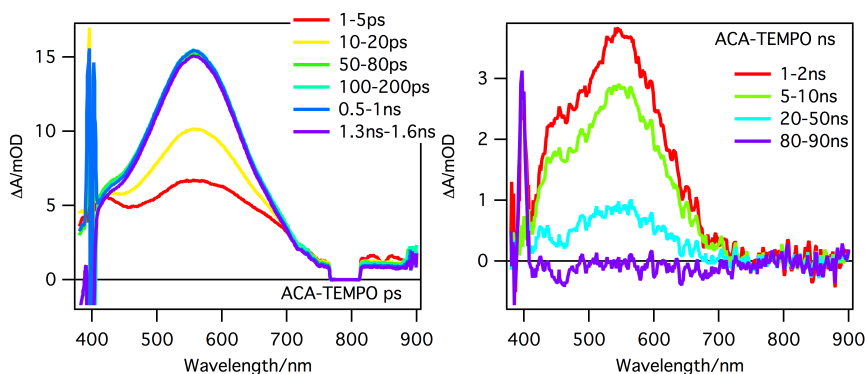
Figure 32: Transient absorption spectra for ACA-TEMPO at picosecond (left) and nanosecond

(right) timescale.

We attempted to use the 840 nm kinetics as the pure singlet signal and 430 nm as a

combined signal of singlet and triplet, yet the triplet kinetics data had large-scale noise and was

thus not successful. Our interpretation of this result is that a charge transfer process occurred

instead of ISC. As shown in Figure 33, since the TEMPO radical was attached in close proximity

to the center of the anthracene, electron transfer between the anthracene and TEMPO is likely

resulting in a reduced anthracene anion and an oxidized TEMPO cation. This interpretation is

supported by the fact that the transient absorption spectrum of anthracene anion peak appears at

550 nm, which is consistent with our experimental result (Figure 33).

ACA-TEMPO S_1

ACA-TEMPO T_1

ACA$^+$ -TEMPO$^-$
ACA$^-$ -TEMPO$^-$
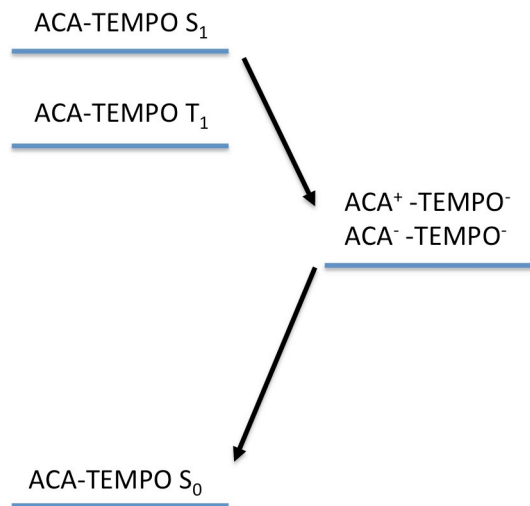
ACA-TEMPO S_0

Figure 33: An illustration of possible charge transfer process for ACA-TEMPO

3.3 Conclusion

In summary, the anthracene system displays an interesting ISC. The anthracene skeleton, without any modifications, exhibits ISC. Modifying the anthracene with thiol groups increases the ISC rate and decreases the triplet lifetime. The preliminary conclusion of the EISC exhibited by ACA-SH is that this is generated from a radical-like effect due to the partial dissociation of S-H bond, and a modification involving linking a thiol group introduces very minor structural changes which do not influence the electronic and energy orbitals, which minimizes other processes such as charge transfer. When covalently linked with TEMPO radical, however, anthracene does not show EISC. Instead, charge transfer takes places which generates a reduced anthracene anion and an oxidized TEMPO cation.

Appendix

This appendix contains additional information regarding to the experiment results discussed in

Chapter 2 and 3.
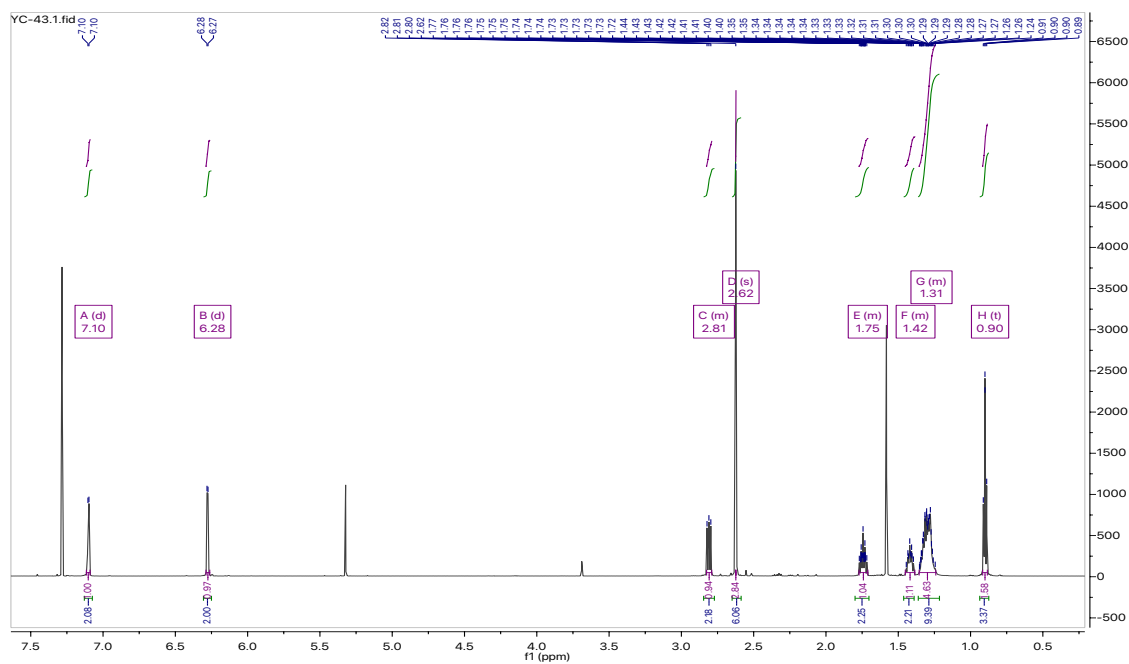
Figure A. 1: ^{1}H NMR of the fundamental BODIPY skeleton for BDP-TEMPO-S and

BDP-TEMPO-L synthesis
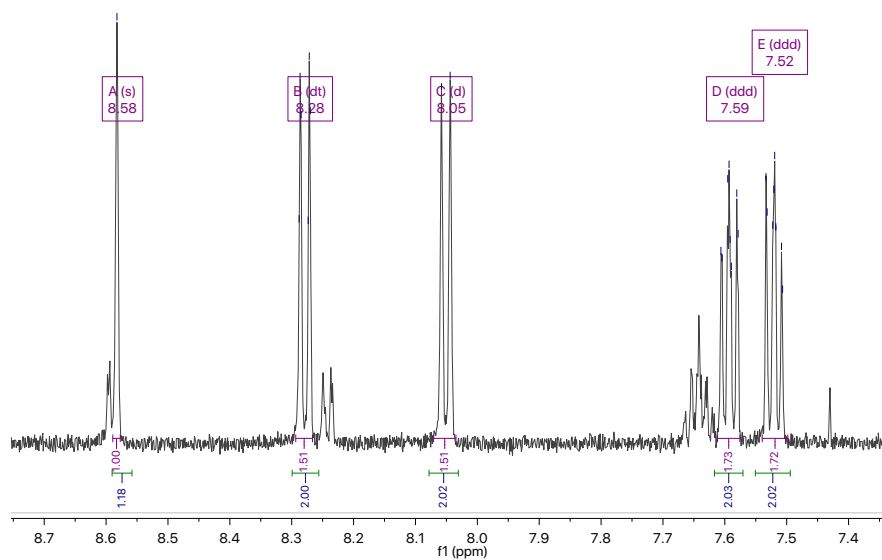
Figure A. 2: The ^{1}H NMR for antracene-9-acid chloride, an intermediate for ACA-TEMPO

synthesis.

Bibliography

1. Abdullah, N. R.; Tang, C.-S.; Manolescu, A.; Gudmundsson, V., Cavity-Photon Controlled Thermoelectric Transport through a Quantum Wire. *ACS Photonics* **2016,** *3* (2), 249-254.

2. Zhao, J.; Wu, W.; Sun, J.; Guo, S., Triplet photosensitizers: from molecular design to applications. *Chemical Society Reviews* **2013,** *42* (12), 5323-5351.

3. Wang, Z.; Zhao, J.; Barbon, A.; Toffoletti, A.; Liu, Y.; An, Y.; Xu, L.; Karatay, A.; Yaglioglu, H. G.; Yildiz, E. A.; Hayvali, M., Radical-Enhanced Intersystem Crossing in New Bodipy Derivatives and Application for Efficient Triplet–Triplet Annihilation Upconversion. *Journal of the American Chemical Society* **2017,** *139* (23), 7831-7842.

4. Awuah, S. G.; You, Y., Boron dipyrromethene (BODIPY)-based photosensitizers for photodynamic therapy. *RSC Advances* **2012,** *2* (30), 11169-11183.

5. Yersin, H., Triplet Emitters for OLED Applications. Mechanisms of Exciton Trapping and Control of Emission Properties. In *Transition Metal and Rare Earth Compounds: Excited States, Transitions, Interactions III*, Springer Berlin Heidelberg: Berlin, Heidelberg, 2004; pp 1-26.

6. Gorman, A.; Killoran, J.; O'Shea, C.; Kenna, T.; Gallagher, W. M.; O'Shea, D. F., In Vitro Demonstration of the Heavy-Atom Effect for Photodynamic Therapy. *Journal of the American Chemical Society* **2004,** *126* (34), 10619-10631.

7. Prier, C. K.; Rankic, D. A.; MacMillan, D. W. C., Visible Light Photoredox Catalysis with Transition Metal Complexes: Applications in Organic Synthesis. *Chemical Reviews* **2013,** *113* (7),

5322-5363.

8.   Romero, N. A.; Margrey, K. A.; Tay, N. E.; Nicewicz, D. A., Site-selective arene C-H amination via photoredox catalysis. *Science* **2015,** *349* (6254), 1326.

9.   Forrest, S. R.; Thompson, M. E.; Baldo, M. A., Intersystem crossing agents for efficient utilization of excitons in organic light emitting devices. Google Patents: 2001.

10. Colvin, M. T.; Giacobbe, E. M.; Cohen, B.; Miura, T.; Scott, A. M.; Wasielewski, M. R., Competitive Electron Transfer and Enhanced Intersystem Crossing in Photoexcited Covalent TEMPO−Perylene-3,4:9,10-bis(dicarboximide) Dyads: Unusual Spin Polarization Resulting from the Radical−Triplet Interaction. *The Journal of Physical Chemistry A* **2010,** *114* (4), 1741-1748.

11. Filatov, M. A.; Karuthedath, S.; Polestshuk, P. M.; Savoie, H.; Flanagan, K. J.; Sy, C.; Sitte, E.; Telitchko, M.; Laquai, F.; Boyle, R. W.; Senge, M. O., Generation of Triplet Excited States via Photoinduced Electron Transfer in meso-anthra-BODIPY: Fluorogenic Response toward Singlet Oxygen in Solution and in Vitro. *Journal of the American Chemical Society* **2017,** *139* (18), 6282-6285.

12. Chernick, E. T.; Casillas, R.; Zirzlmeier, J.; Gardner, D. M.; Gruber, M.; Kropp, H.; Meyer, K.; Wasielewski, M. R.; Guldi, D. M.; Tykwinski, R. R., Pentacene Appended to a TEMPO Stable Free Radical: The Effect of Magnetic Exchange Coupling on Photoexcited Pentacene. *Journal of the American Chemical Society* **2015,** *137* (2), 857-863.

13. Sun, Z.; Wu, J., Open-shell polycyclic aromatic hydrocarbons. *Journal of Materials Chemistry* **2012,** *22* (10), 4151-4160.

14. Qu, H.; Chi, C., A Stable Heptacene Derivative Substituted With Electron-Deficient Trifluoromethylphenyl and Triisopropylsilylethynyl Groups. *Organic Letters* **2010,** *12* (15), 3360-3363.

15. Gao, X.; Hodgson, J. L.; Jiang, D.-e.; Zhang, S. B.; Nagase, S.; Miller, G. P.; Chen, Z., Open-Shell Singlet Character of Stable Derivatives of Nonacene, Hexacene and Teranthene. *Organic Letters* **2011,** *13* (13), 3316-3319.

16. Colvin, M. T.; Giacobbe, E. M.; Cohen, B.; Miura, T.; Scott, A. M.; Wasielewski, M. R., Competitive Electron Transfer and Enhanced Intersystem Crossing in Photoexcited Covalent TEMPO– Perylene-3, 4: 9, 10-bis (dicarboximide) Dyads: Unusual Spin Polarization Resulting from the Radical– Triplet Interaction. *The Journal of Physical Chemistry A* **2010,** *114* (4), 1741-1748.

17. Ishii, K.; Hirose, Y.; Fujitsuka, H.; Ito, O.; Kobayashi, N., Time-Resolved EPR, Fluorescence, and Transient Absorption Studies on Phthalocyaninatosilicon Covalently Linked to One or Two TEMPO Radicals. *Journal of the American Chemical Society* **2001,** *123* (4), 702-708.

18. Shie, J.-J.; Liu, Y.-C.; Lee, Y.-M.; Lim, C.; Fang, J.-M.; Wong, C.-H., An Azido-BODIPY Probe for Glycosylation: Initiation of Strong Fluorescence upon Triazole Formation. *Journal of the American Chemical Society* **2014,** *136* (28), 9953-9961.

19. Wu, K.; Chen, J.; McBride, J. R.; Lian, T., Efficient hot-electron transfer by a plasmon-induced interfacial charge-transfer transition. *Science* **2015,** *349* (6248), 632.

20. Taghinejad, M.; Taghinejad, H.; Xu, Z.; Liu, Y.; Rodrigues, S. P.; Lee, K. T.; Lian, T.; Adibi, A.; Cai, W., Hot-Electron-Assisted Femtosecond All-Optical Modulation in Plasmonics. *Advanced Materials* **2018,** *30* (9), 1704915.

21. Huang, J.; Huang, Z.; Jin, S.; Lian, T., Exciton Dissociation in CdSe Quantum Dots by Hole Transfer to Phenothiazine. *The Journal of Physical Chemistry C* **2008,** *112* (49), 19734-19738.

22. Nakatsuji, S. i.; Ojima, T.; Akutsu, H.; Yamada, J.-i., Anthracene Derivatives and the Corresponding Dimers with TEMPO Radicals. *The Journal of Organic Chemistry* **2002,** *67* (3), 916-921.

23. Livingston, R.; Tanner, D. W., The triplet state of anthracene in liquid solutions. *Transactions of the Faraday Society* **1958,** *54*, 765-771.